University of Stavanger

GURVEER SINGH
SUPERVISOR: REMUS GABRIEL HANEA

Reservoir Optimization through Data-Space Inversion

A comparative Analysis and Practical Evaluation

Master thesis, 2024

Energy, Reservoir and Earth Sciences

Faculty of Science and Technology

Department of Energy Resources

University of Stavanger

FACULTY OF SCIENCE AND TECHNOLOGY

MASTER'S THESIS

Study programme/specialisation: Energy, Reservoir and Earth Sciences	Spring semester, 2024 Open
Author: Gurveer Singh	
Supervisor(s): Remus Gabriel Hanea	
Title of master's thesis: Reservoir Optimization through Data Space Inversion: A Comparative Analysis and Practical Evaluation	
Credits: 30	
Keywords: Data space inversion, data-driven models, ES-MDA, ensemble based optimization	Number of pages: 62 Stavanger, 15/06/2024

Acknowledgement

This thesis is submitted as part of the MSc degree requirements in Energy, Reservoir, and Earth Sciences at the Faculty of Science and Technology, Department of Energy Resources, University of Stavanger (UiS). This thesis was done in collaboration with Equinor ASA.

First and foremost, I would like to express my heartfelt gratitude to my supervisor, Professor Remus Gabriel Hanea. Thank you for introducing me to this topic and providing support whenever and wherever needed. I would like to thank Eduardo Barros and Slawomir Szklarz, researchers from TNO, for providing valuable insight into their work and technical scholarly support for mine.

I would like to express my gratitude to Subhi Sadigov, Reservoir Engineer at Equinor, for his assistance in helping with Fast Model Update (FMU) setup and providing guidance in overcoming any obstacles encountered. I am very grateful to Torill Halland, my line manager at Equinor, for assisting me with the logistical issues, as well as Tobias Müller, who was the project manager for this project.

A big thanks to my wife, Arpita Chaturvedi, for supporting and helping me throughout my MSc, as well as to my sweet daughter, Anureet, whose face was all I needed for my stress to go away and start working with new vigor. Lastly, I extend my heartfelt gratitude to my parents, who have consistently supported my decisions throughout my ambitious pursuits.

G.S.

Abstract

Ensemble-based reservoir management procedures have become the standard when it comes to uncertainty quantification; this in turn has resulted in increased processing requirements, which are not only time-consuming but can also negatively impact the economics of the projects. To mitigate the problems posed by conventional methods in such cases, researchers have shifted their focus to data-driven approaches that could prove to be robust, computationally inexpensive, and effective while dealing with closed-loop reservoir management.

These direct forecasting techniques have shown enormous potential, and data space inversion (DSI) is one such technique. DSI conditions its predictions using historically observed data. This study presents the implementation of DSI using Ensemble Smoother with Multiple Data Assimilation (ES-MDA) and an optimization tool using a stochastic simplex approximate gradient. Both tools used for ES-MDA and optimization are mature tools with large-scale commercial applications. The optimization and sensitivity are performed on a synthetic field, Drogon, selected specifically due to its realistic characteristics.

The entire workflow was implemented based on two different sets of observations. The predictions are conditioned on their respective observations and are then compared to the synthetic truths. These results are then optimized along with the synthetic truths. In both cases, the DSI ensemble prediction and optimization results have an acceptable match with their respective truths, thus establishing the viability and robustness of the DSI technique. In the DSI framework, one can choose specific properties to predict, which eliminates the time-consuming calculation of redundant properties.

The results confirm the huge potential of this technique, especially when used in closed-loop reservoir management, providing us with efficient, inexpensive, and accurate predictions for decision-making.

Table of Contents

Acknowledgement i

Abstract ii

Table of Contents iii

List of Tables v

List of Figures v

Abbreviations x

1 Introduction 1

1.1 Background . . . 1
1.2 Objectives . . . 3
1.3 Outline . . . 4

2 Theory 5

2.1 Reservoir Management . . . 5
2.1.1 History Matching . . . 5
2.1.2 Optimization . . . 6
2.2 DSI . . . 10
2.2.1 Auto Encoder . . . 10
2.2.2 Building DSI with ES-MDA and Autoencoder . . . 12
2.2.3 Differences between history matching and optimization with DSI . . . 15

3 Methodology 17

3.1 Reservoir Model . . . 17
3.2 Workflow . . . 21

3.2.1 Optimization Problem Formulation . . . 21
3.2.2 'Truth', DSI Prior and Prosterior . . . 22
3.2.3 Running Optimization . . . 22
3.2.4 NPV Comparison . . . 23
3.2.5 Repeat for a different 'truth' . . . 23
3.2.6 Sensitivity Study . . . 23

4 Results and Discussion **26**
4.1 DSI Results: 'truth-1' . . . 26
4.1.1 History Match Results . . . 26
4.1.2 Prediction Results . . . 29
4.2 Optimization Results: 'truth-1' . . . 30
4.3 Sensitivity Results . . . 31
4.3.1 Sensitivity on Prior Size . . . 32
4.3.2 Sensitivity on Observation Error . . . 34
4.3.3 Sensitivity on Latent Space . . . 37
4.4 DSI Results Comparison for 'truth-1' and 'truth-2' . . . 40
4.5 Optimization Results: 'truth-2' . . . 42

5 Conclusions **45**
5.1 Conclusions . . . 45
5.2 Recommendations for Further Work . . . 46

References **47**

Appendix **49**

List of Tables

3.1 Zones and range of uncertain properties distribution for the Drogon reservoir model (Equinor, a). . . . 18
3.2 This table represents NPV Computation Parameters. . . . 22
3.3 Observation Error Sensitivity . . . 24

4.1 NPV for initial and optimized cases for 'truth-1'. . . . 31
4.2 Initial and optimal injection rates in m3/day for 'truth-1'. . . . 32
4.3 NPV for initial and optimized cases for 'truth-2'. . . . 44
4.4 Initial and optimal injection rates in m3/day for 'truth-2'. . . . 44

List of Figures

2.1 Schematic representation of the stochastic optimization technique for a simple two control problem (Equinor, b) . . . 8

2.2 General structure of an autoencoder (Michelucci, 2022) . . . 11

2.3 Effect of reconstruction error on the output. (Michelucci, 2022) . . . 13

2.4 Schematic representation of conventional history matching (left) and data space inversion (right) workflows, adapted from Szklarz and Barros (2022) . . . 15

2.5 Schematic representation of DSI based closed-loop approach, adapted from Szklarz and Barros (2022) . . . 16

3.1 Facies Concept for Drogon (Equinor, a). . . . 18

3.2 Well configuration for Drogon. . . . 19

3.3 Drogon 'truth' model initial oil saturation distribution. . . . 19

3.4 Relative permeability and capillary pressure curves for Drogon. (Equinor, a) . . . 20

3.5 Plots showing prediction of initial ensemble with 100 realizations. . . . 20

3.6 The main workflow of master's thesis. . . . 21

4.1 Plots showing oil production rates for each producer. Red dots are observed data, grey envelope is the prior ensemble, and blue envelope is posterior ensemble of DSI predictions. The darker shades within the envelope show 25-75 percentile of their respective ensembles. . . . 27

4.2 Plots showing water production rates for each producer. Red dots are observed data, grey envelope is the prior ensemble, and blue envelope is posterior ensemble of DSI predictions. The darker shades within the envelope show 25-75 percentile of their respective ensembles. . . . 27

4.3 Plots showing BHP for each producer. Red dots are observed data, grey envelope is the prior ensemble, and blue envelope is posterior ensemble of DSI predictions. The darker shades within the envelope show 25-75 percentile of their respective ensembles. 28
4.4 Plots showing water injection rates of injectors A5 & A6. Red dots represent the observed data 28
4.5 Plots showing oil production for each producer. Black dots are 'truth-1' predictions, grey envelope is the prior ensemble, and blue envelope is posterior ensemble of DSI predictions. The darker shades within the envelope show 25-75 percentile of their respective ensembles. 29
4.6 Plots showing water production for each producer. Black dots are 'truth-1' predictions, grey envelope is the prior ensemble, and blue envelope is posterior ensemble of DSI predictions. The darker shades within the envelope show 25-75 percentile of their respective ensembles. 30
4.7 Plots showing water injection of both the injectors. Black dots are 'truth-1' predictions, grey envelope is the prior ensemble, and blue envelope is posterior ensemble of DSI predictions. The darker shades within the envelope show 25-75 percentile of their respective ensembles. 30
4.8 Chart showing NPV comparison between three scenarios 31
4.9 Plots show comparisons between control parameters for three cases for both injectors. 32
4.10 Figures show oil production for producer A-1 for prior sizes of 200, 500 and 1000. Black dots are 'truth-1' predictions, grey envelope is the prior ensemble, and blue envelope is posterior ensemble of DSI predictions. The darker shades within the envelope show 25-75 percentile of their respective ensembles. 33
4.11 Figures show water production for producer A-1 for prior sizes of 200, 500 and 1000. Black dots are 'truth-1' predictions, grey envelope is the prior ensemble, and blue envelope is posterior ensemble of DSI predictions. The darker shades within the envelope show 25-75 percentile of their respective ensembles. 33
4.12 Figures show water injection for injector A-5 for different latent space. Black dots are 'truth' predictions, grey envelope is the prior ensemble, and blue envelope is posterior ensemble of DSI predictions. The darker shades within the envelope show 25-75 percentile of their respective ensembles. 34
4.13 Figures show oil production rate for producer A-2 for different sets of observation error. Red dots are observed data, grey envelope is the prior ensemble, and blue envelope is posterior ensemble of DSI predictions. The darker shades within the envelope show 25-75 percentile of their respective ensemble. 35

4.14 Figures show water production rate for producer A-2 for different sets of observation error. Red dots are observed data, grey envelope is the prior ensemble, and blue envelope is posterior ensemble of DSI predictions. The darker shades within the envelope show 25-75 percentile of their respective ensemble. 35

4.15 Figures show BHP of producer A-2 for different sets of observation error. Red dots are observed data, grey envelope is the prior ensemble, and blue envelope is posterior ensemble of DSI predictions. The darker shades within the envelope show 25-75 percentile of their respective ensembles. 36

4.16 Figures show oil production for producer A-2 for different sets of observation error. Black dots are 'truth-1' predictions, grey envelope is the prior ensemble, and blue envelope is posterior ensemble of DSI predictions. The darker shades within the envelope show 25-75 percentile of their respective ensemble. 36

4.17 Figures show water production for producer A-2 for different sets of observation error. Black dots are 'truth-1' predictions, grey envelope is the prior ensemble, and blue envelope is posterior ensemble of DSI predictions. The darker shades within the envelope show 25-75 percentile of their respective ensembles. 37

4.18 Figures show oil production rate for producer A-1 for different latent space. Red dots are observed data, grey envelope is the prior ensemble, and blue envelope is posterior ensemble of DSI predictions. The darker shades within the envelope show 25-75 percentile of their respective ensembles. 38

4.19 Figures show water production rate for producer A-1 for different latent space. Red dots are observed data, grey envelope is the prior ensemble, and blue envelope is posterior ensemble of DSI predictions. The darker shades within the envelope show 25-75 percentile of their respective ensembles. 38

4.20 Figures show BHP for producer A-1 for different latent space. Red dots are observed data, grey envelope is the prior ensemble, and blue envelope is posterior ensemble of DSI predictions. The darker shades within the envelope show 25-75 percentile of their respective ensembles. 39

4.22 Figures show water production for producer A-3 for different latent space. Black dots are 'truth-1' predictions, grey envelope is the prior ensemble, and blue envelope is posterior ensemble of DSI predictions. The darker shades within the envelope show 25-75 percentile of their respective ensembles. 39

4.21 Figures show oil production for producer A-1 for different latent space. Black dots are 'truth-1' predictions, grey envelope is the prior ensemble, and blue envelope is posterior ensemble of DSI predictions. The darker shades within the envelope show 25-75 percentile of their respective ensembles. 40

4.23 Figures show oil and water production rate and BHP of producer A-1 for different truth. Red dotted line represent the observed data, grey envelope represents the prior ensemble, dark grey area shows 25-75 percentile of prior ensemble. Blue envelope shows posterior ensemble. 41
4.24 Figures show water injection of injector A5 for different truth. Black dots are 'truth' predictions, grey envelope is the prior ensemble, and blue envelope is posterior ensemble of DSI predictions. The darker shades within the envelope show 25-75 percentile of their respective ensembles. 42
4.25 Figures show oil and water production of producer A-1 for different truth. Black dots are 'truth' predictions, grey envelope is the prior ensemble, and blue envelope is posterior ensemble of DSI predictions. The darker shades within the envelope show 25-75 percentile of their respective ensembles. 42
4.26 Chart showing NPV comparison between three scenarios 43
4.27 Plots shows comparison between optimal control parameters for three cases for both the injectors 43

A.1 Injection control variables attained from from Everest-ECL across multiple optimization iterations over four time periods for 'truth-1' 49
A.2 Injection control variables attained from from Everest-DSI across multiple optimization iterations over four time periods for 'truth-1' 49
A.3 Injection control variables attained from from Everest-ECL across multiple optimization iterations over four time periods for 'truth-2' 50
A.4 Injection control variables attained from from Everest-DSI across multiple optimization iterations over four time periods for 'truth-2' 50

Abbreviations

AE	-	Auto Encoder
AHM	-	Assisted History Matching
BHP	-	Bottom Hole Pressure
DSI	-	Data Space Inversion
DSIVC	-	Data Space Inversion Variable Control
DST	-	Drill Stem Test
HM	-	History Matching
EnKF	-	Ensemble Kalman Filter
EOR	-	Enhanced Oil Recovery
ES	-	Ensemble Smoother
ES-MDA	-	Ensemble Smoother Multiple Data Assimilation
FOPR	-	Field Oil Production Rate
FOPT	-	Field Oil Production Total
FWIR	-	Field Oil Injection Rate
FWIT	-	Field Oil Injection Total
IOR	-	Improved Oil Recovery
MSE	-	Mean Square Error
NPV	-	Net Present Value
QC	-	Quality Check
RE	-	Reconstruction Error
RF	-	Recovery Factor
ROI	-	Rate on Investment
StoSAG	-	Stochastic Simplex Approximate Gradient
WOPR	-	Well Oil Production Rate
WOPT	-	Well Oil Production Total
WWIR	-	Well Water Injection Rate
WWIT	-	Well Water Injection Total
WWPR	-	Well Water Production Rate
WWPT	-	Well Water Production Total

Chapter 1

Introduction

This opening chapter presents brief explanation of the motivation behind this master's thesis and its objectives.

1.1 Background

The first stage in oil and gas development is primary recovery with the support of natural drive mechanisms present in the reservoir. As the reservoir pressure decreases due to oil production, the reservoir's natural driving mechanism becomes incapable of supporting an efficient and economically attractive oil recovery; hence, a secondary recovery method is used. Waterflooding is the most widely used secondary recovery method to increase oil production and the ultimate hydrocarbon. Injected water helps to retain the pressure in the long run and displaces the oil towards the producers, thus resulting in improved sweep efficiency. Most often, optimization studies are conducted to find the optimal well control settings for producers and injectors that maximize net present value (NPV), or the ultimate hydrocarbon recovery. Coupling a numerical simulator with an optimization algorithm requires a significant number of computationally expensive dynamic simulations, which is a time-consuming and expensive procedure.

The complexity of modeling and simulating producing fields increases significantly when these fields are subjected to advanced Improved Oil Recovery (IOR) and Enhanced Oil Recovery (EOR) techniques. In such scenarios, conventional simulation models become prohibitively expensive and computationally demanding. DSI emerges as a technique that can substantially reduce the computational expense of these simulations, offering a more efficient alternative. Thus, providing a method that can handle the challenging computational issues faced by the oil and

gas sector, especially important as we move towards more intricate recovery procedures and look for ways to optimize the resources that are already in place.

DSI is a technique that can predict the model's outcomes either for history matching (HM) or future predictions using statistical models or machine learning without running the reservoir models. DSI emerged from the literature on weather forecasting and uses ensemble simulation and data methodologies, thus avoiding the computationally demanding task of continuously modifying the physical reservoir model (Oliver et al., 2008). A Bayesian DSI framework for calculating the posterior probability distribution of the entire data space on observed data was described by Sun and Durlofsky (2017), Jiang et al. (2020). However, the suggested methodology only selects prior models that closely resemble actual responses, potentially ignoring valuable information from excluded models, and requires complex mapping procedures for forecasting non-Gaussian variables. In the existing methods, posterior predictions are typically generated for a specific set of well controls, but Jiang et al. (2020) proposed a new technique called Data Space Inversion Variable Control (DSIVC). It eliminates the requirement to re-simulate all previous models and enables posterior predictions with user-defined well control parameters. Thus, allowing quick posterior prediction and great computing economy. In closed-loop optimization in uncertain scenarios, DSIVC also shows a significant reduction in uncertainty.

Later, Lima et al. (2020) introduced DSI using an ensemble smoother. For an actual field with a long production history, they were able to estimate the output forecast with success. Forecasts from the novel DSI approach were on par with those from more conventional ensemble-based history matching methods.

Szklarz and Barros (2022) presented the implementation of the DSI framework using the ES-MDA method available within Ensemble Reservoir Tool (ERT), an open-source data assimilation tool. They confirmed that DSI has the potential to be an appropriate technique for optimization workflows with variable controls and investigated its further potential within closed-loop reservoir management framework. Additionally, Szklarz and Barros (2022) examined how different data conditioning strategies were used and found that autoencoders are a great option for managing extremely non-linear data. Autoencoders are considered an excellent option because most data pertaining to real oilfields is non-linear.

In this thesis, the author will implement the DSI framework using ES-MDA technique, leveraging the open-source data assimilation tool Ensemble Reservoir Tool (ERT) and the industry-standard optimization tool EVEReST, with the main endeavor of testing the DSI technique, evaluating its accuracy against recognized reservoir models, and assessing its robustness. Our objective is to achieve the desired reservoir optimization results and compare these outcomes with those obtained through conventional methods using Eclipse and EVEReST. The exercise will be

conducted on the synthetic field, Drogon, known for its realism and suitability as a stepping-stone for real field implementation. This comparison will provide valuable insights into the efficiency and effectiveness of the DSI technique in optimizing reservoir performance and its potential application in real oilfields.

1.2 Objectives

The objective of the thesis is to offer a detailed insight into the DSI technology, evaluate its accuracy against recognized reservoir models, assess its potential across a range of reservoir circumstances, and handling uncertainties. The further scope of this thesis is to evaluate the robustness of this technology across a range of reservoir circumstances and complicated geological aspects.

The following tasks are performed to achieve the main objective of this thesis:

1. Generate a prior with different controls to cover the possible field conditions using ECLIPSE.
2. Generate the DSI posterior ensemble and predictions based on the prior generated from the ECLIPSE as input.
3. Define and formulate the optimization problem to be solved.
4. Optimize the DSI ensemble and find the optimal control.
5. Use conventional optimization on the truth case and find the optimal NPV.
6. Find the optimal control variable configuration corresponding to the maximum NPV obtained from closed-loop optimization with DSI.
7. Using the numerical reservoir simulator, simulate the observed case with the optimal injection rate control settings obtained from DSI and calculate the NPV.
8. Compare the values of the NPV to check the validity of the DSI optimization.
9. Repeat the process of optimization using DSI, calculate the NPV using the optimal DSI controls and conventionally optimized NPV for new truth, and compare the results to establish its robustness.
10. Use DSI to calculate the new posterior using varying observation errors, different latent spaces of the autoencoder, and varying prior sizes.
11. Compare the results of all the sensitivity analyses.

1.3 Outline

The rest of the thesis contains the following sections in chronological order:

- Chapter 2. Theory: presents theories and principles used in this study, including literature studies and how they are relevant.
- Chapter 3. Methodology: presents the project workflow, showing how the tasks were approached to reach the main objective and the setup for optimization problem solved in this study.
- Chapter 4. Results and Discussion: presents and discusses the findings and outcomes of the optimization performed using DSI and the results of optimization runs.
- Chapter 5. Conclusion and Recommendation for Further Work: this chapter sums up the most important findings based on the results obtained and provides ideas for further research.

Chapter 2

Theory

This chapter presents the underlying theories and principles used in this study, including literature reviews and their relevance to this study. This chapter covers aspects of reservoir management, including history matching, field development optimization, and data space inversion.

2.1 Reservoir Management

2.1.1 History Matching

Assisted History Matching (AHM), or data assimilation, is the process through which the reservoir model is adjusted based on the observed data of the field. This data could be production data, bottom hole pressure (BHP), drill stem test (DST) data, or any other data recorded in the field. The foundation of the AHM is based on the Ensemble Kalman Filter (EnKF), which was first introduced by Evensen (1994). Since its introduction, it has been used in various fields, like meteorology, oceanography, and reservoir engineering. Oliver and Chen (2011) summarizes the main developments of EnKF in AHM. Additionally, they talked about the concept of the ensemble smoother (ES) for AHM, which is one of the simplified approaches that updates the model parameters in a single step. However, dealing with non-linearities can be challenging and could lead to unrealistic updates.

Emerick and Reynolds (2013) proposed ES-MDA and addresses these limitations by employing multiple data assimilation steps, resulting in more stable, convergent, and accurate history matching. In this study, DSI framework is implemented using ES-MDA.

2.1.2 Optimization

Optimization is the process of generating the maximum value for the stakeholders while taking into account various constraints. It covers well placements, well schedules, well controls (production/injection rates), and other elements to optimize the recovery while minimizing emissions and maximizing profits. In reservoir engineering, optimization on the ensemble is referred to as robust optimization. This approach utilizes optimization on an ensemble that represents the various possible scenarios in which a reservoir could perform, including the associated risks and uncertainties. In reservoir management, optimization with ensemble-based modelling offers a more robust, flexible, and dependable approach.

An ensemble generates a range of possible scenarios, but robust optimization on the ensemble yields a single optimal strategy. We can define our objective function, and based on it, we can derive an optimal strategy that achieves our goal. Objective function could be maximizing the NPV, minimizing the CO_2, or well-path optimization etc.

All the optimization techniques could be divided into two main categories: derivative-based and derivative-free techniques.

Derivative-based Optimization Techniques

Derivative-based methods involves calculating the gradients or higher-order derivatives of the objective function with respect to the required variables. Gradient descent and Newton-Raphson are two specific examples of such methods. These methods yield results quickly and efficiently when the objective function is smooth and differentiable. However, they could struggle to resolve complex, non-smooth, or highly non-linear problems that typically occur in reservoirs.

Derivative-free Optimization Techniques

Derivative-free methods don't need to compute gradients or higher-order derivatives and can handle a wider range of optimization problems, including complex, non-smooth, or highly non-linear problems. Genetic algorithms and particle swarm optimization are some of the examples of these techniques. These techniques could solve complex problems and find global maxima or minima, but they take longer to converge and require more processing power.

Brouwer and Jansen (2004) discuss the application of both gradient-based methods and alternative approaches in the optimization of water flooding in reservoir management. It provides

insights into how these techniques are applied in the industry and compares their effectiveness. While Onwunalu and Durlofsky (2010) discusses the use of particle swarm optimization, a derivative-free method, for well placement and well type determination, highlighting its advantages and computational challenges in reservoir engineering.

These optimization techniques can be used in different aspects of reservoir management depending on the problem, as both these techniques offer different benefits and limitations. Nevertheless, due to the complex nature of reservoirs and the high computational demands, gradient-based methods are more commonly employed.

This study uses Everest, which is an industry-standard tool and is built upon the computationally efficient derivative/gradient-based methods. Chen et al. (2009) introduced ensemble-based optimization based on an approximate gradient-based method, and Fonseca et al. (2016) proposed stochastic gradient-based optimization and these could be termed the foundation of optimization performed in this study .

This method begins by selecting an initial set of controls. For example, in Fig. 2.1, the point (u1 = -1, u2 = 0) has been chosen as the initial controls. Around the initial controls, Everest generates a set of perturbed controls that have a normal distribution, depicted as blue dots in Fig. 2.1. The objective function value for each of these blue dots is then evaluated, represented by the red dots. With this information, the gradient of the objective function can be approximated. The gradient estimate at the initial point is obtained by performing a linear regression through the red dots, resulting in the green line. A simple line-search algorithm is then employed to take a step in the gradient direction, leading to an "updated" set of controls. This process is repeated until convergence is achieved, indicated by minimal or no change in the objective function. (Equinor, b).

Stochastic Simplex Gradient

Fonseca et al. (2016) introduced the stochastic simplex approximate gradient (StoSAG) as an optimization technique to obtain precise approximate gradients when working with ensemble of models containing varying parameters for uncertainty quantification. This method is independent of the number of control variables and generates the gradients stochastically by sampling within a simplex—a geometric object made up of n+1 vertices in an n-dimensional space. Optimization tool Everest supports StoSAG formulation for estimating the gradient in robust optimization problems (Equinor, b).

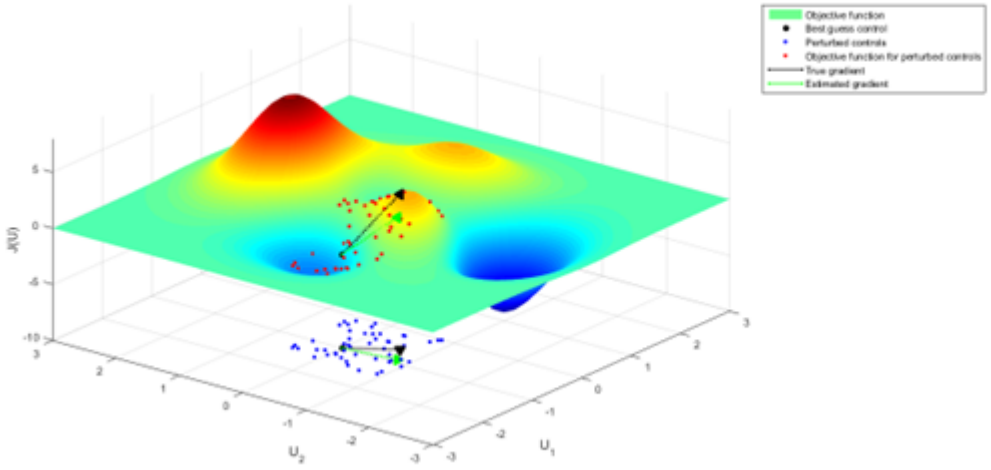

Figure 2.1: Schematic representation of the stochastic optimization technique for a simple two control problem (Equinor, b)

Objective Function[1]

The objective function is the most important part of the optimization, as all the operations are performed either to maximize or minimize the objective function while considering all the constraints. For example, when dealing with net present value, we must optimize our controls to maximize the value of the objective function, whereas when dealing with CO_2 emissions, we must optimize controls so that the objective function is minimized.

Following are some of the commonly used objective functions denoted by J:

- NPV
- Return on investment (ROI)
- Recovery factor (RF)
- CO_2 emission
- Water injection/production

The objective function reaches its optimum value by modifying the controls while remaining within the constraints (c). Production and Injection rate limits, BHP limits, well drillability are some of the common constraints. The objective function is defined by Eq. 2.1.

[1]This section is adapted and modified from lecture notes of GEO608 course at UiS (Haena, 2023).

$$J(u) = f(u, m) \tag{2.1}$$

where, u is the controls and m is selected realization from the ensemble.

In a robust optimization, we find a single strategy that is optimal across all the model realization as presented by Eq. 2.2.

$$u_{rob} = arg\max_{u} \bar{J(u)} \tag{2.2}$$

where, u_{rob} is robust optimization controls and $\bar{J}$ is mean objective function which is calculated using Eq. 2.3.

$$\bar{J(u)} = \frac{1}{N}\sum_{i}^{N} J(u, m_i) \tag{2.3}$$

where, N is the number of ensemble members and ensemble M_{ens} can be presented as:

$$M_{ens} = \{m_1, m_2, m_3, ..., m_N\}$$

and, m_1, m_2, m_N are model realizations realizations.

When handling multi-objective optimization, such as the concurrent maximisation of NPV and minimization of emissions, the significance of each individual objective function is determined, and weights are allocated accordingly.

Considering w_1 and w_2 to be the respective weights of objective functions J_1 and J_2, then the final objective function will look like the following:

$$J(u) = w_1 \cdot J_1(u) + w_2 \cdot J_2(u) \tag{2.4}$$

Where J_1 and J_2 are different objective functions and w_1 and w_2 are their associated weights.

In this thesis, the author uses NPV as the objective function while considering revenue from oil, injection costs, and water production costs. The author does not account for the initial cost of investment when calculating the NPV. The final NPV is calculated using Eq. 2.5:

$$NPV = \sum_{n=0}^{N} \frac{(R_{o,n} - C_{i,n} - C_{p,n})}{(1+r)^n} \tag{2.5}$$

Where, $R_{o,n}$ is the revenue from oil production at time n, $C_{i,n}$ is the injection cost at time n, $C_{p,n}$

is the production cost at time n, r is the discount rate, and N is the time-period in years.

The revenue from oil production $R_{o,n}$ can be calculated from Eq. 2.6:

$$R_{o,n} = P \times Q_n \tag{2.6}$$

Here, P is the oil price per unit, Q_n is the quantity of oil produced at time n.

The annual production cost $C_{p,n}$ can be calculated from Eq. 2.7:

$$C_{p,n} = C \times Q_n \tag{2.7}$$

where C is the cost of oil production per unit.

The injection cost $C_{i,n}$ can be calculated from Eq. 2.8:

$$C_{i,n} = I \times W_n \tag{2.8}$$

where I is the cost of water injection per unit, W_n is the quantity of water injected at time n.

2.2 DSI

DSI approaches aim to establish a statistical correlation between the observed and forecast variables as well as to quantify the predictive uncertainty of the forecast variables, by using an ensemble of uncalibrated prior models.

2.2.1 Auto Encoder

Autoencoders (AE) were first introduced by Rumelhart et al. (1986) in 1986. Autoencoder is an algorithm that learns from a data representation and encodes it into a latent space from where it can be reconstructed and used further for different application. It is a type of artificial neural network and is mainly used for dimension reduction or feature learning (Bank et al., 2020).

Autoencoder consists of three main components: an encoder, latent space, and a decoder (Michelucci, 2022). In this study, author has used autoencoder for dimension reduction so that Ensemble Smoother Multiple Data Assimilation (ES-MDA) can handle complex non-linear data. General

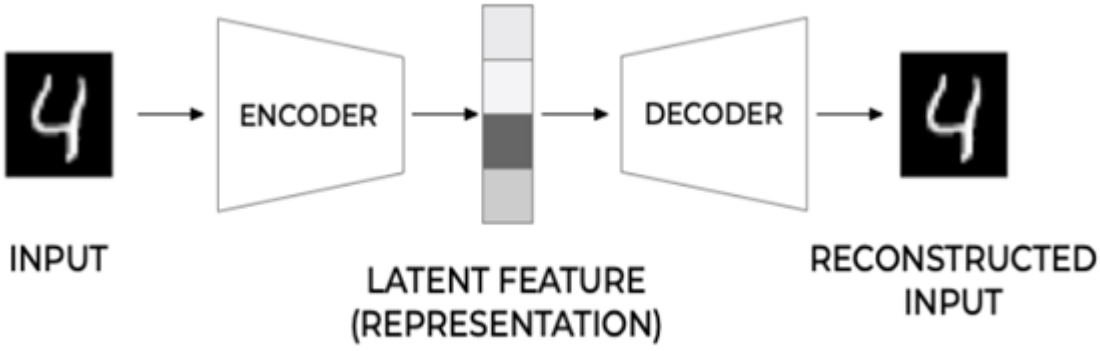

Figure 2.2: General structure of an autoencoder (Michelucci, 2022)

structure of AE is depicted in Fig. 2.2.

Encoder :

It takes the input data and converts it into the lower-dimensional representation. Encoders are typically neural network layers and can easily be trained with existing resources (Michelucci, 2022).

Decoder :

Decoder takes the encoded representation and attempts to reconstruct the original data, trying to make the final data as close as to original data as possible.

Latent Space :

The encoder's output represents the latent space and plays an essential role in data reconstruction. The optimum latent space dimension is one of the most crucial features to be considered. If we deem it to be too small, then our final output will lack crucial attributes; if we choose it to be too big, then our computational time will be too large, compromising the efficiency of the entire process.

Encoder can be written as a function, and if the input data is x_i and encoder is g and the latent representation is denoted by h, then an individual element of the latent representation h_i can be given by Eq. 2.9:

$$h_i = g(x_i) \tag{2.9}$$

and if the decoder is denoted by f and the reconstructed data is denoted by $\overline{x}$ then the final reconstructed data element $\tilde{x_i}$ can be written by expression in Eq.2.10:

$$\tilde{x_i} = f(h_i) = f(g(\tilde{x_i})) \tag{2.10}$$

Training autoencoder involves finding functions f and g that minimize the difference between x_i and $\tilde{x_i}$. When presented in the form of a function it is called loss function and the objective is to minimize this function. Loss function can be written as such (Eq:2.11):

$$arg\min_{f,g} < [\Delta(x_i, f(g(x_i))] \tag{2.11}$$

The most commonly used loss function is mean square error (MSE).

Reconstruction error (RE) is another method that gives us the quality of reconstruction data from the input observation. The most typically used RE is mean square error (MSE) (Eq: 2.12). The bigger the error the poor quality of the reconstructed data and vice versa. Effect of the reconstruction can be shown by Fig. 2.10. It can be observed that higher the error, the poor the quality of the reconstructed results.

$$RE = MSE = \frac{1}{M}\sum_{i=1}^{M} |x_i - \tilde{x_i}|^2 \tag{2.12}$$

Here. M is the number of observations.

2.2.2 Building DSI with ES-MDA and Autoencoder

Szklarz and Barros (2022) presented implementation of DSI using following steps:

1. **Data Preparation**:
   The geological ensemble is simulated with initial control settings to get the predictions of the initial ensemble. Datasets of historical observations, model parameters, and different control scenarios are also collected.

2. **Prepare DSI prior**:
   For each ensemble member, simulate the reservoir model for aforementioned different control scenarios to obtain forecasted data D^f.

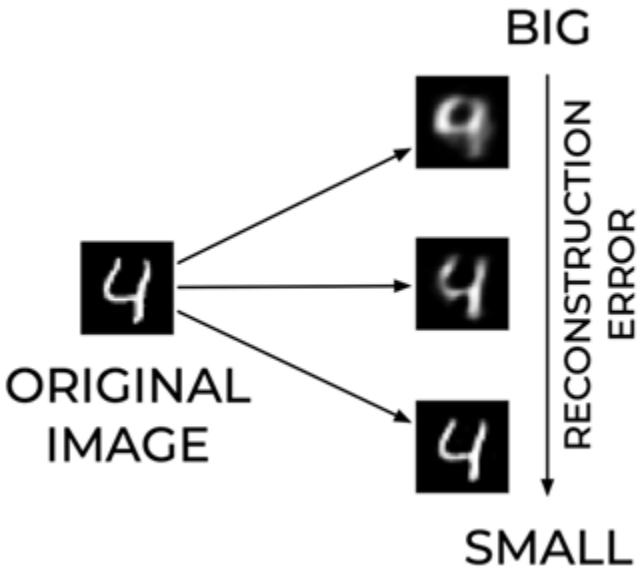

Figure 2.3: Effect of reconstruction error on the output. (Michelucci, 2022)

3. **Latent Space Transformation**:
   Transform the observed data (d) and observed control variables (c) into latent space using Eq. 2.13.

$$z = Encoder(d, c) \tag{2.13}$$

   where z is latent space representation of the observed data and controls. Transform the forecasted data and control variables into the latent space using Eq. 2.14.

$$Z^f = Encoder(D^f, C) \tag{2.14}$$

   where C is control variables used in the simulation, and Z^f is latent space representation of the forecasted data.
   For the initial condition, equation will be written as Eq. 2.15

$$Z^o = Encoder(D^o, C) \tag{2.15}$$

   where Z^o is the latent space representation of the initial ensemble data, and D^o is initial ensemble of data.

4. **Perturb observed data**:
   Perturb the latent space representation of the observed data and controls for each ensemble member using Eq. 2.16.

$$z_i^k = z + \epsilon_i^k \tag{2.16}$$

where z_i^k is perturbed latent space representation of the observed data for the ensemble member i at step k, and ϵ_i^k is error added to the observed data for realization i at step k.

5. **Calculate Covariance in Latent Space**:
   Compute the covariance matrix of the latent space forecasted data (including controls) C_{zz} using Eq. 2.17.
   $$C_{zz} = \frac{1}{n}(Z^f - \overline{Z}^f)(Z^f - \overline{Z}^f)^T \tag{2.17}$$
   where $\overline{Z}^f$ is the mean of forecasted latent space data.

6. **Calculate Klaman Gain**:
   Kalman gain is calculated using Eq. 2.18
   $$K_k = C_{ZZ}(C_{ZZ} + \alpha_k C_\epsilon)^{-1} \tag{2.18}$$
   here, α_k is a parameter that controls the step size or the weight of the update in each assimilation step, and C_ϵ is the covariance matrix of the observation noise in the latent space.

7. **Update Ensemble Members**:
   Each member of ensemble are then updated using Eq. 2.19
   $$z_i^{\alpha,k} = z_i^f + \alpha_k K_k(z_i^k - z_i^f) \tag{2.19}$$

8. Repeat the forecast and assimilation steps for $k = 1, 2, ...n$

9. **Reconstruction**:
   Once the assimilation is completed, use the decoder part of the autoencoder to transform the updated latent space data back to the original data to get the final results.

After obtaining the data, it can be used in the Everest for optimizations. It is pertinent to note that the data controls in the DSI steps are global controls while the controls in the Everest are local controls updated through perturbations. The DSI will serve as the forward model in the Everest, and predictions will be generated from the DSI framework without the need to simulate the geological models.

2.2.3 Differences between history matching and optimization with DSI

Figure 2.4 depicts comparison among conventional history matching and DSI-AE based history matching (Szklarz and Barros, 2022).

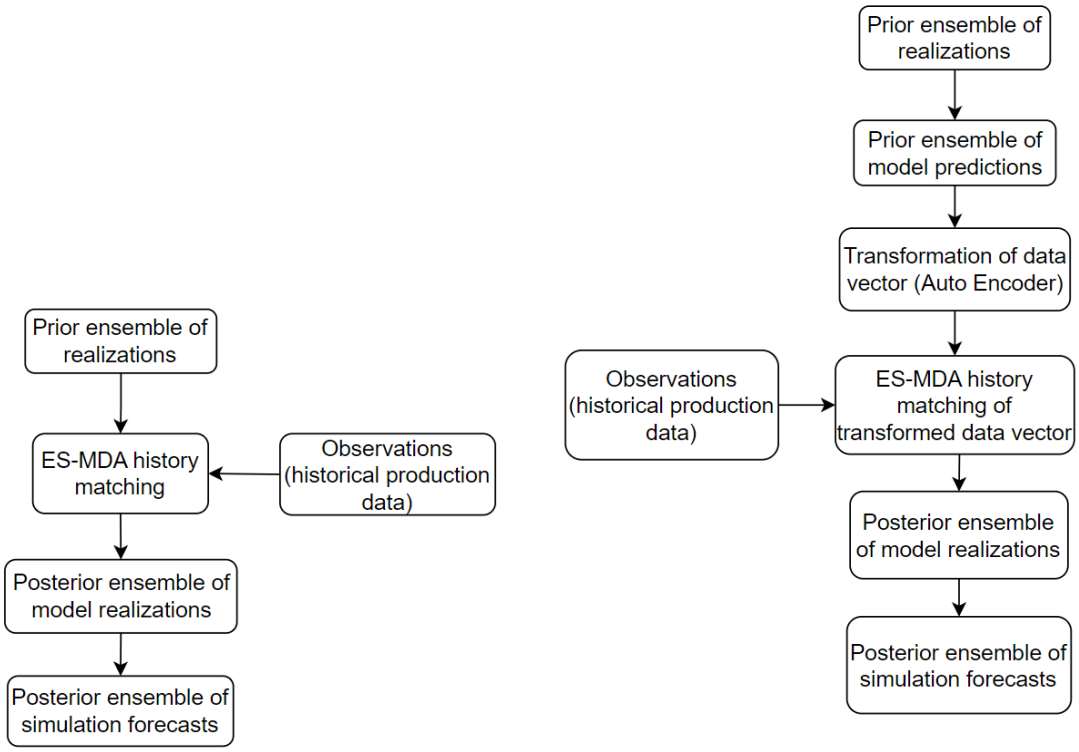

(a) Conventional HM **(b)** DSI-AE based HM

Figure 2.4: Schematic representation of conventional history matching (left) and data space inversion (right) workflows, adapted from Szklarz and Barros (2022)

Szklarz and Barros (2022) developed a workflow as shown in Fig. 2.5 for DSI based closed-loop reservoir management. This workflow uses DSI forecasts for optimization study. This workflow allows combining the optimization in a closed-loop framework with DSI by incorporating control variables in a forecast period together with simulated data and predictions in the vector to be updated in DSI.

Firstly, one geological model is removed from the ensemble and referred to as 'truth', it is used to produce synthetic observations. Then the remaining ensemble is simulated to generate prior ensemble of model predictions. These are further transformed into a data vector using Auto Encoder. ES-MDA assisted history matching of this transformed vector results in posterior en-

semble of realizations which are further simulated to get the forecasts.

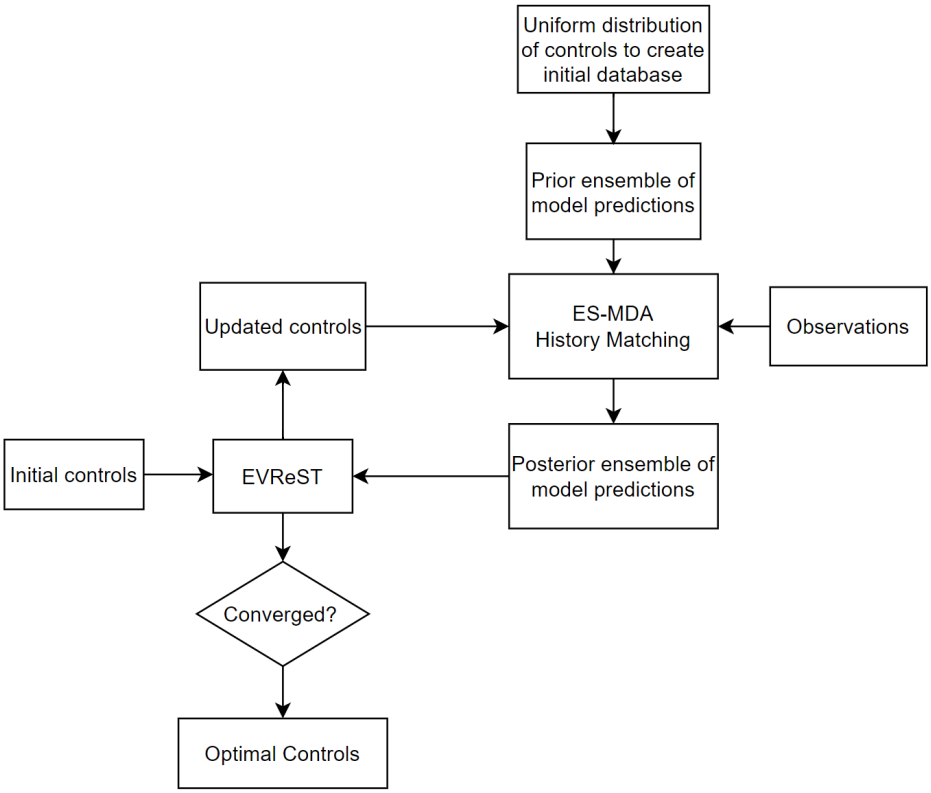

Figure 2.5: Schematic representation of DSI based closed-loop approach, adapted from Szklarz and Barros (2022)

Chapter 3

Methodology

This chapter presents how the DSI technique described in the previous chapter is used to perform injection rate optimization without a conventional simulator. Following section presents and discusses the details of the reservoir model used for this study.

3.1 Reservoir Model

Drogon, a synthetic model developed by Equinor, has been choosen to test the workflow described in the next section and accomplish the objective of this study. Drogon is a synthetic reservoir model, a successor to the Reek Field, which was also developed by Equinor.

According to the conceptual description (Equinor, a), the reservoir belongs to the Volantis group and consists of three formations: Valysar, Therys, and Volon. The Valysar is a fluvial system featuring channel bodies, with a predominant presence of continuous coal at its the lower boundary. The four facies are channel bodies, crevasse, overbank, and coals.

Therys is a shoreline system grading from shoreface facies to offshore facies with the presence of calcite-cemented strings. The shoreline strike direction is close to the north-south, and in the east, parts of the reservoir are missing. The Volon is a braided fluvial system with the presence of calcites intervals. The top boundary seems to be dominated by extensive calcite. The channel strike direction is interpreted to be close to north-south, but this is uncertain.

The reservoir is 12000 ft × 15000 ft × 450 ft and is spatially discretized into 46 × 73 × 31 cells. There are in total 100 model realizations to incorporate geological uncertainty. The model con-

Table 3.1: Zones and range of uncertain properties distribution for the Drogon reservoir model (Equinor, a).

Zone	Porosity Range	Permeability Range [mD]
Valysar	0.01-0.33	0.001-1962
Therys	0.01-0.36	0.001-2340
Volon	0.01-0.30	0.001-4446

sists of grid cells with dimensions of approximately 260 ft × 205 ft × 14 ft each. The model has 107,456 cells, out of which 71,475 are active. The Facies concept in Drogon is depicted in Fig. 3.1. The reservoir comprises eight distinct facies that have been modeled in different zones, as tabulated in Table 3.1.

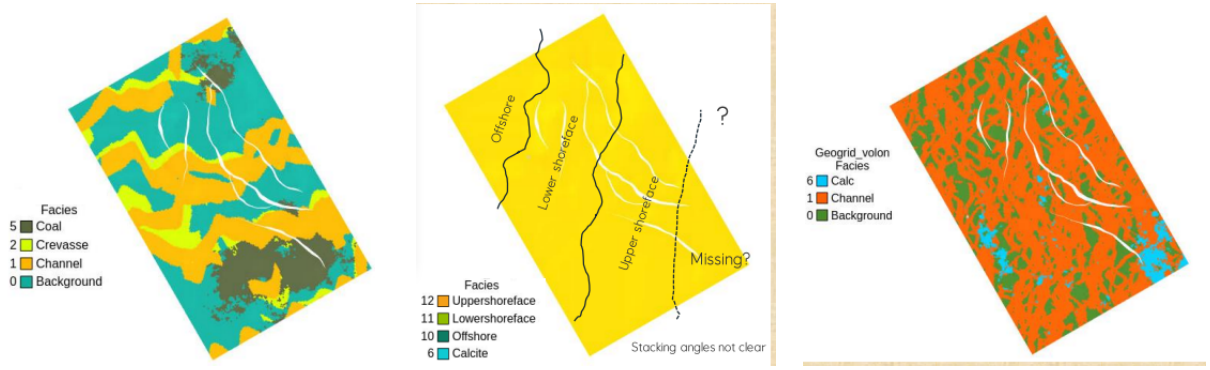

(a) Valysar **(b)** Therys **(c)** Volon

Figure 3.1: Facies Concept for Drogon (Equinor, a).

The reference strategy consists of 4 producers and 2 injectors also shown in Fig. 3.2. Figure 3.3 represents top view visualization of Drogon model.

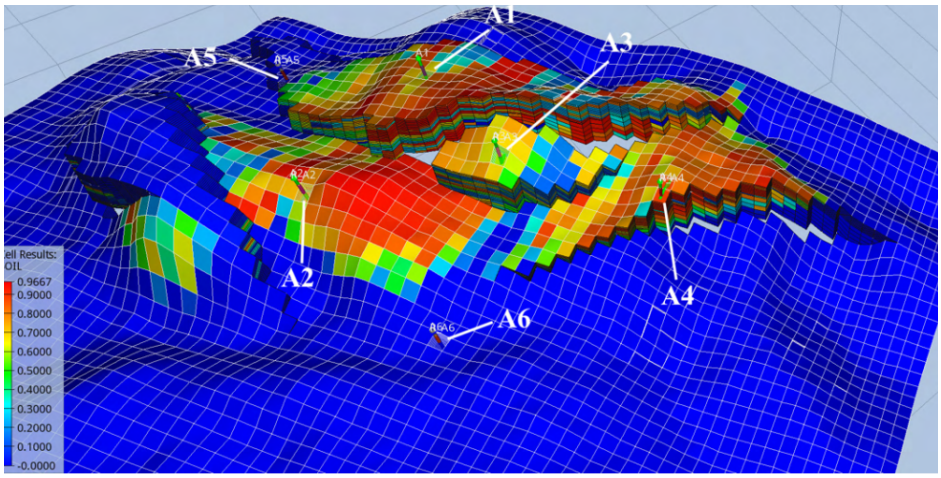

Figure 3.2: Well configuration for Drogon.

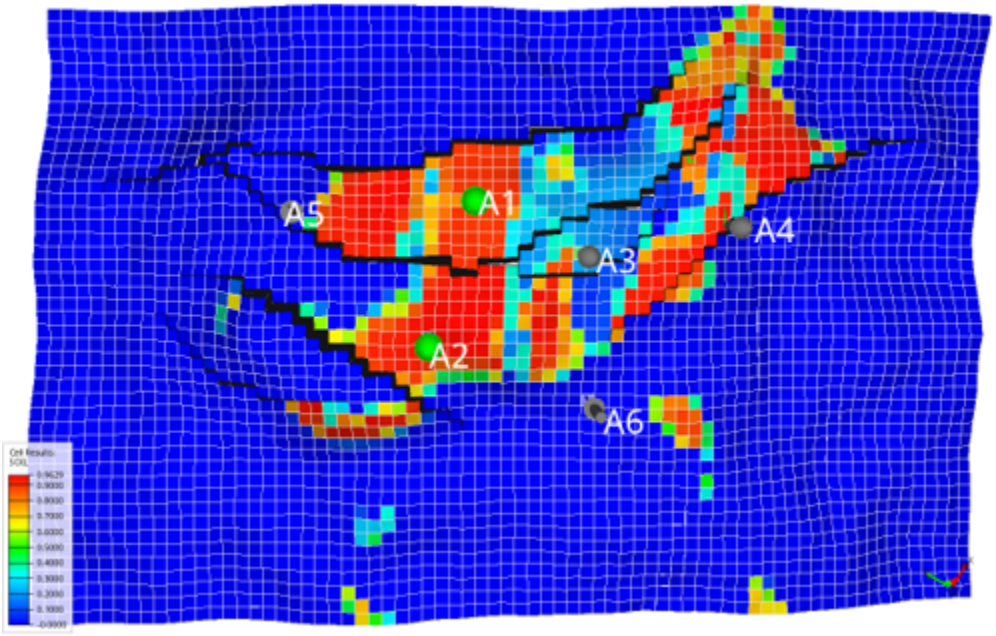

Figure 3.3: Drogon 'truth' model initial oil saturation distribution.

The presence of 12 saturation tables (SATNUMs) with different relative permeability curves further reflects the complexity of the reservoir, as shown in Fig. 3.4. Figure 3.5 illustrates the Field Oil Production Rate (FOPR), Field Water Production Rate (FWPR), Field Gas Production Rate (FGPR) and Field Water Injection Rate (FGIR) of the initial ensemble of Drogon with 100 geological realizations.

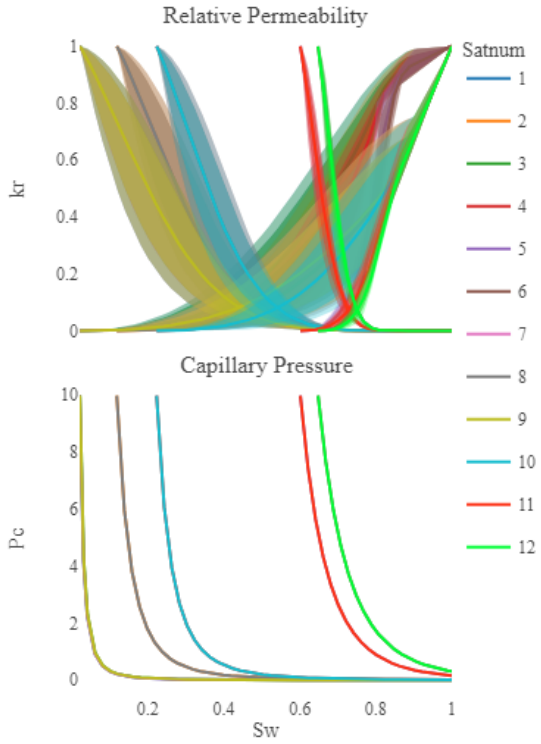

Figure 3.4: Relative permeability and capillary pressure curves for Drogon. (Equinor, a)

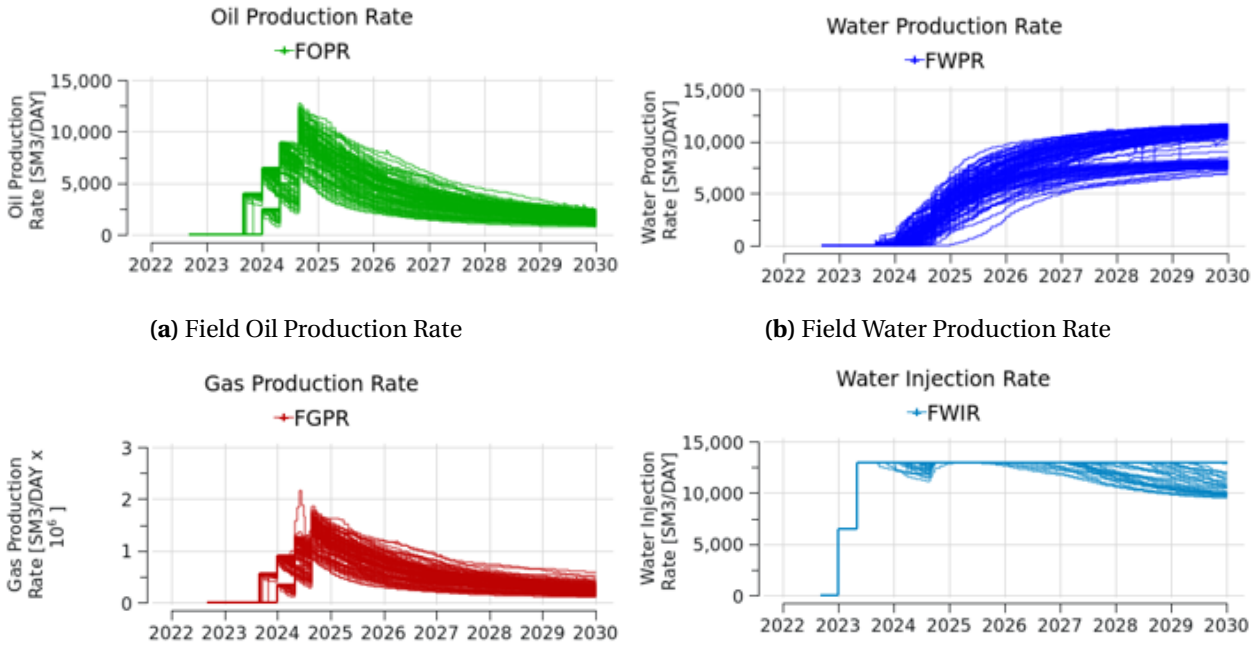

(a) Field Oil Production Rate

(b) Field Water Production Rate

(c) Field Gas Production Rate

(d) Field Water Injection Rate

Figure 3.5: Plots showing prediction of initial ensemble with 100 realizations.

3.2 Workflow

Figure 3.6 shows the main workflow of this master's thesis. The steps are discussed in detail below.

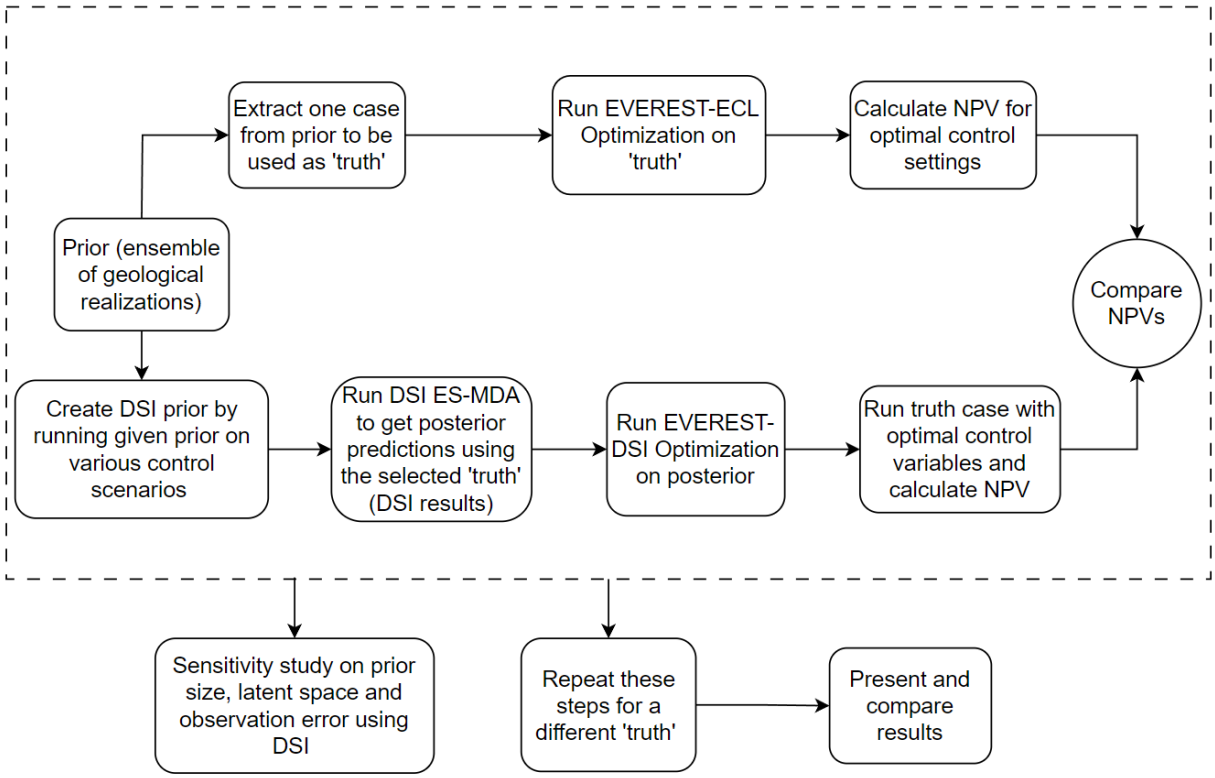

Figure 3.6: The main workflow of master's thesis.

3.2.1 Optimization Problem Formulation

The Drogon field lifespan for this project is 7 years, from January 2023 until January 2030. This period is divided into historical and prediction periods. The time period from January 2023 to October 2025 is simulated in historical mode, and the rest of the period is simulated in prediction mode. Historical properties or observed data include Well Bottom Hole Pressure (WBHP), Well Oil Production Rate (WOPR), Well Water Production Fate (WWPR), and Well Water Injection Rate (WWIR). Historical data is given on a quarterly basis, resulting in a total of 12 time steps.

This work focuses on the optimization of the water injection rate of the two injectors, A-5 and A-6. The objective function that we are optimizing is the NPV. Equation 2.5 mentioned in section 2.1.2 is used to calculate NPV.

Table 3.2 presents some important parameters used in the NPV computation. The oil price chosen here is not representative of the current market but is slightly on the conservative side.

A maximum well injection rate constraint of 10,000 m^3/day is imposed, and the changes to the well injection rate can be made only once per year. Thus, considering two injectors and four control variables for each injector, the total number of control variables amounts to 8. Subsequently, the optimum injection rates are obtained using DSI-EVEREST optimization to get the maximum NPV.

Table 3.2: This table represents NPV Computation Parameters.

Type	Value
Oil price ($/Sm3)	340
Cost produced water ($/Sm3)	12
Cost injected water ($/Sm3)	6.29
Annual discount factor	0.08
End of life cycle period (years)	7

3.2.2 'Truth', DSI Prior and Prosterior

As discussed in the previous section, this study uses 100 geological realizations as a starting point, also referred to as prior. One geological realization is removed from the prior, referred to as 'truth-1', and is used to produce observed data.

This approach allows us to compare the predictions with the 'truth-1', as these predictions are not used in any form beyond the historical period. Thus, it can serve as a invaluable tool for quality checking, especially when working with newer techniques such as DSI.

A new prior is created for DSI by running the ensemble on various controls using the conventional simulator. It is the only time when a conventional simulator is used in the entire DSI workflow. It is crucial to emphasize that the prior does not include the 'truth-1'.

The DSI workflow presented in Fig. 2.4(b) is used to obtain the posterior ensemble of predictions.

3.2.3 Running Optimization

The 'truth-1' is used for comparing the optimization results. Firstly, the 'truth-1' is optimized using Eclipse and Everest, and the optimal NPV is calculated, referred to as $NPV_{\text{Everest-ECL}}$. Af-

terwards, Everest-DSI optimization is run on the posterior to get the optimal control variables. The 'truth-1' case is simulated with the optimal control variable obtained from Everest-DSI optimization, and $NPV_{\text{Everest-DSI}}$ is then calculated to provide comparison with the conventional optimization method.

The main advantage of computationally efficient DSI framework is that it eliminates the need for model updates for the predictions.

3.2.4 NPV Comparison

As stated in the previous section, two optimized NPV, $NPV_{\text{Everest-ECL}}$ and $NPV_{\text{Everest-DSI}}$, are obtained from conventional optimization and DSI-based optimization, respectively. Both NPVs are then compared to check the performance of Everest-DSI optimization. NPV_{initial} is also calculated using the forecasts obtained by simulating the 'truth-1'.

3.2.5 Repeat for a different 'truth'

To confirm the validity of the DSI workflow, the entire exercise is repeated for a new truth ('truth-2'). This is done to quality-check (QC) the DSI performance. First, a new 'truth' is selected, and then to check the robustness of the technique, the entire workflow is repeated. Concurrently, the 'truth-2' is also optimized using Eclipse and Everest, and the corresponding optimal NPV is calculated. Furthermore, the DSI posterior ensemble of predictions is optimized using DSI and Everest. Optimal controls are obtained from it, and these optimal controls from the DSI are used on the 'truth-2' to calculate the NPV.

3.2.6 Sensitivity Study

A sensitivity study on prior size, observation error, and latent space dimension is performed to determine the optimal parameters for the current DSI framework.

Prior Size Sensitivity

The prior that is used in the DSI is created by generating the possible outcomes for the controls. If there are 5 sets of controls, the prior size will be 5n, where n represents the number of ensemble members in the the geological model.

The Drogon ensemble used for this study consists of 100 geological realizations. To check the impact of the prior size on the posterior, different priors are created for 2, 5, and 10 control scenarios, resulting in DSI prior with 200, 500 and 1000 members, respectively. Author conducts this exercise to determine the optimal number of prior members, ensuring the model's computational effectiveness and coverage of associated uncertainties.

Observation Error

The observation error plays a significant role in AHM. The low observation error will give a closer match between the posterior ensemble and the observations, conversely, a higher error will give the opposite results. An extremely close match will reduce the model's ability to capture uncertainty, while a larger observation error will assimilate incorrect observations, thereby capturing the wrong uncertainties. Therefore, achieving the right balance between precision and robustness is the key.

To determine the sensitivity of observation error, three scenarios are considered, as presented in Table 3.3: one scenario has a pressure tolerance limit of 1 bar and oil and water rate tolerance limit of 5 m3/day; the other two scenarios have values of 2 bar and 10 m3/day and 4 bar and 20 m3/day, respectively.

Table 3.3: Observation Error Sensitivity

Case	Tolerance limit of pressure, [bar]	Tolerance in oil and water rate, [m3/day]
1	1	5
2	2	10
3	4	20

Latent Space

The autoenconder is used to encode the high-dimensional data into a latent space on which operations are performed, and then the final results are reconstructed by decoding the data from the latent space. This dimensional reduction facilitates the handling of non-linearities and filters out non-essential information. The latent space dimension has a significant impact on the results. A lower dimensionality of the latent space may result in unsatisfactory outcomes due to the potential loss of data during compaction, whereas a higher dimension will have a negative impact on computational efficiency. Hence, the latent space dimension must be carefully con-

sidered to avoid the loss of important information or a substantial increase in computational time.

The author conducts a sensitivity study on the latent space with dimensions of 100, 300, and 500 to determine the optimum size required for this study.

Chapter 4

Results and Discussion

This chapter presents and discusses the results of injection rate optimization study conducted under the DSI framework using ES-MDA. Initially, the outcomes of both history matching and predictions are presented, followed by the optimization results. Furthermore, the results of sensitivity on different parameters are shown. Finally, the results from quality checking the DSI technique on 'truth-2' are presented. The results are also analysed in detail to provide insights required in order to accomplish the objectives of this study.

4.1 DSI Results: 'truth-1'

This section presents the DSI results for history matching and predictions performed based on 'truth-1'.

4.1.1 History Match Results

In this section, results obtained for 'truth-1'from DSI-based history matching are presented and discussed. Figure 4.1 demonstrates the oil production rates of all the producers during the historical period. The blue region in the plots in Fig. 4.1 shows the posterior of the HM ensemble. It is evident that the observed data aligns with this distribution.

Similarly, in Fig. 4.2 depicting the water production rates, a comparable trend is observed. The posterior appears to be slightly collapsed, but this is due to the characteristics of the Drogon field, which exhibits similar behavior when HM is done using conventional methods.

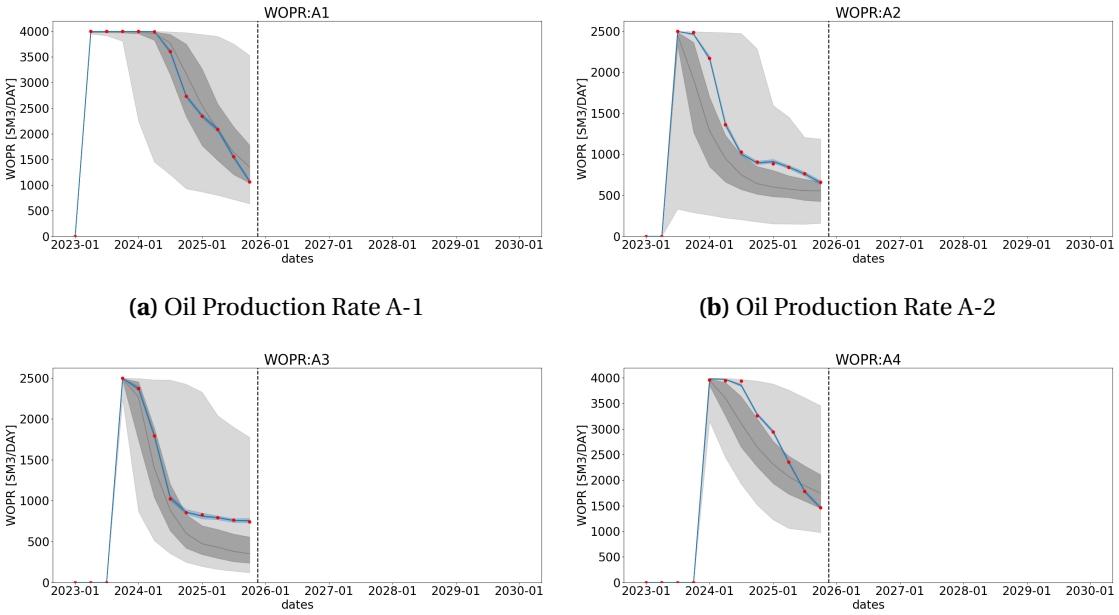

(a) Oil Production Rate A-1

(b) Oil Production Rate A-2

(c) Oil Production Rate A-3

(d) Oil Production Rate A-4

Figure 4.1: Plots showing oil production rates for each producer. Red dots are observed data, grey envelope is the prior ensemble, and blue envelope is posterior ensemble of DSI predictions. The darker shades within the envelope show 25-75 percentile of their respective ensembles.

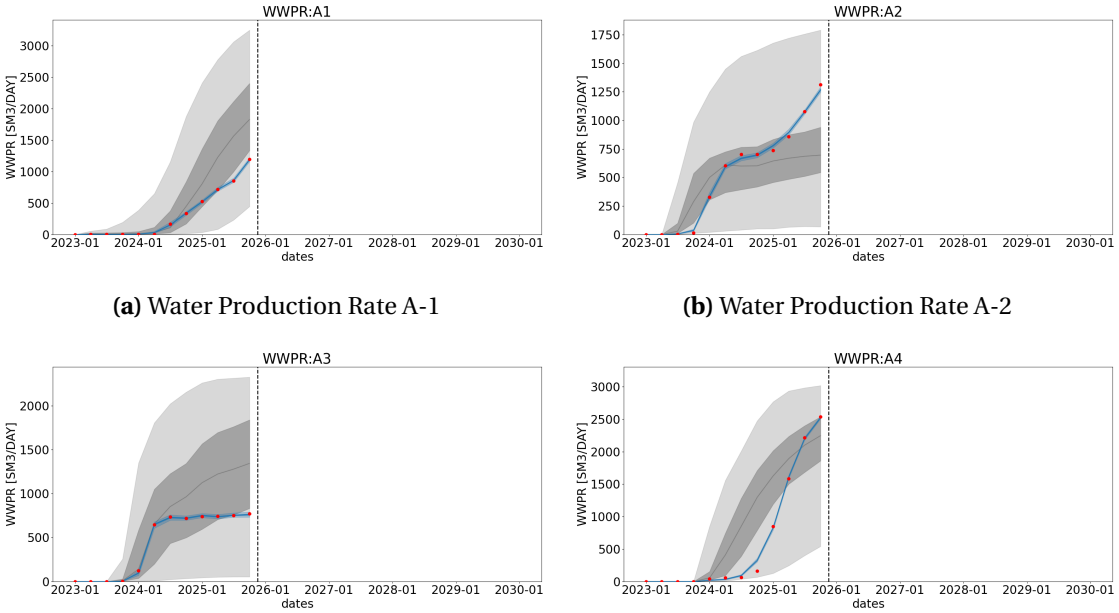

(a) Water Production Rate A-1

(b) Water Production Rate A-2

(c) Water Production Rate A-3

(d) Water Production Rate A-4

Figure 4.2: Plots showing water production rates for each producer. Red dots are observed data, grey envelope is the prior ensemble, and blue envelope is posterior ensemble of DSI predictions. The darker shades within the envelope show 25-75 percentile of their respective ensembles.

Figure 4.3 illustrates the BHP of the producers, and it is evident that the 'truth' lies within the posterior ensemble. Figure 4.4 shows the injection rates, which displays a precise correspondence. This is mostly because the injection rates are constant in the prior used in the DSI.

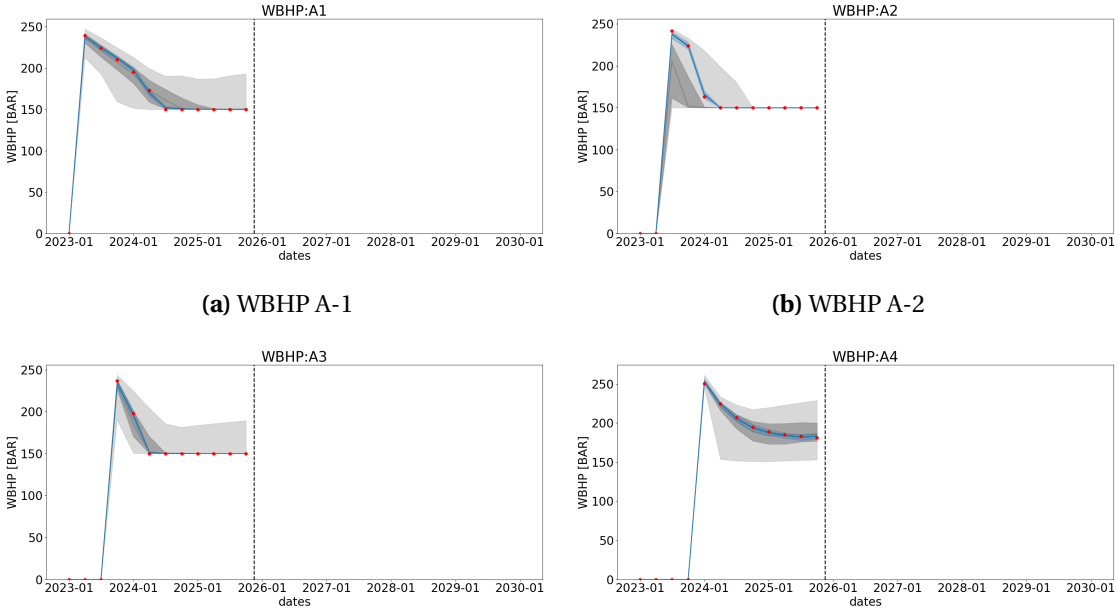

(a) WBHP A-1

(b) WBHP A-2

(c) WBHP A-3

(d) WBHP A4

Figure 4.3: Plots showing BHP for each producer. Red dots are observed data, grey envelope is the prior ensemble, and blue envelope is posterior ensemble of DSI predictions. The darker shades within the envelope show 25-75 percentile of their respective ensembles.

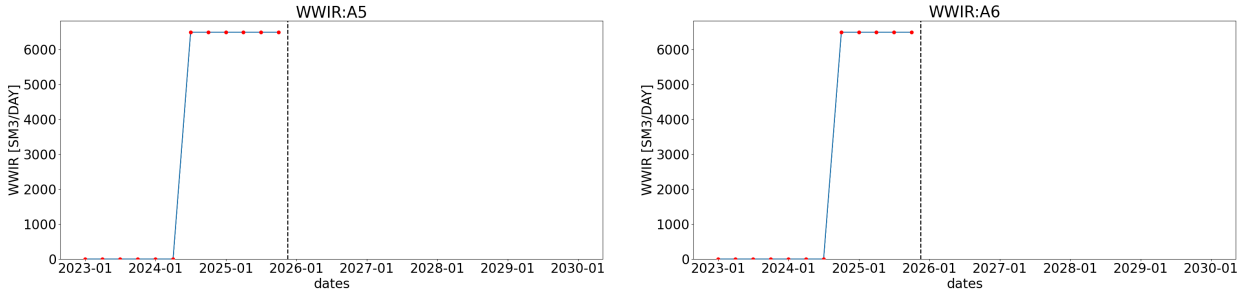

(a) Water Injection Rate A5

(b) Water Injection Rate A6

Figure 4.4: Plots showing water injection rates of injectors A5 & A6. Red dots represent the observed data

The predictions generated by conventional or data-driven techniques rely on conditioning the models using the observed data. Hence, it is crucial for these methods to generate a posterior ensemble that closely aligns with the actual data in order to obtain reliable predictions. Based on the aforementioned results, it can be deduced that the HM (posterior ensemble) is a suitable

fit with the observed data. It is anticipated that the predictions from the DSI framework would yield satisfactory results. The next section discusses forecasts obtained using DSI on ‘truth-1’.

4.1.2 Prediction Results

Figures 4.5, 4.6, 4.7 show the total amount of oil produced, water produced, and water injected for each individual well, respectively. The black dotted line indicates the extension of the ‘truth-1’; however, as previously stated in Chapter 3 in Section 3.2.2, this data is not utilised in any way for prediction. Rather, it is used to demonstrate how closely our posterior ensemble of DSI predictions fits these values, thereby establishing the accuracy of the DSI framework.

The main objective of this study is optimization of injection rates through DSI while maximizing NPV. The NPV is calculated using the predicted values of produced oil, produced water, and injected water. Thus, it is crucial to make precise predictions of these properties. The predicted values from the posterior ensemble of DSI demonstrate a satisfactory level of agreement when compared to the ‘truth-1’. This gives confidence in the deployment of DSI for optimization tasks.

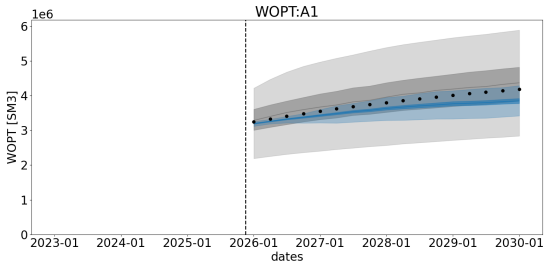

(a) Oil Production for A-1

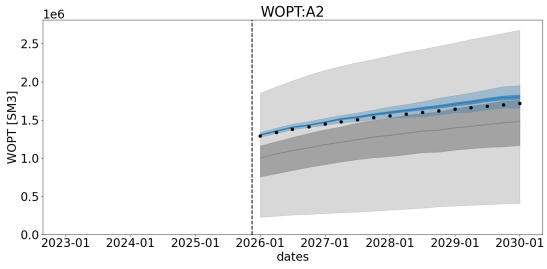

(b) Oil Production for A-2

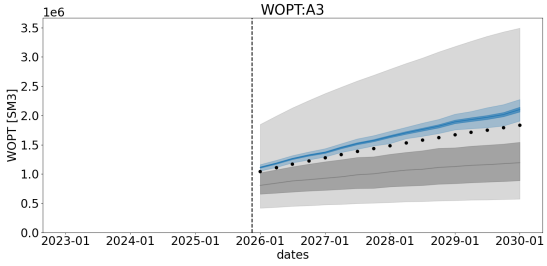

(c) Oil Production for A-3

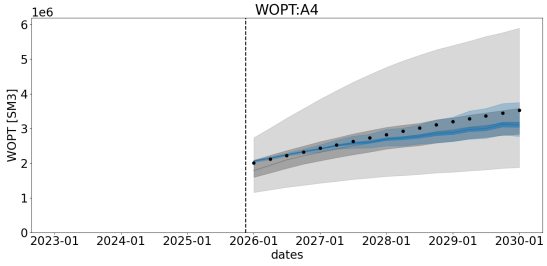

(d) Oil Production for A-4

Figure 4.5: Plots showing oil production for each producer. Black dots are ‘truth-1’ predictions, grey envelope is the prior ensemble, and blue envelope is posterior ensemble of DSI predictions. The darker shades within the envelope show 25-75 percentile of their respective ensembles.

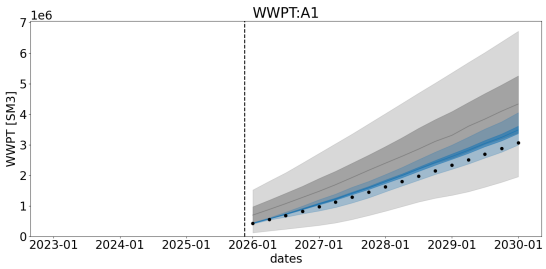

(a) Water Production for A-1

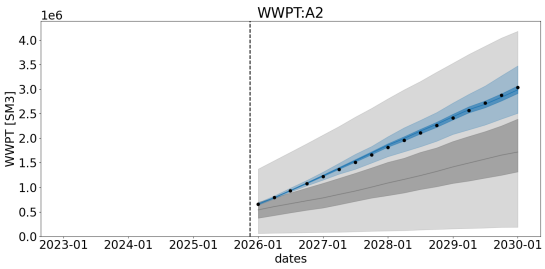

(b) Water Production for A-2

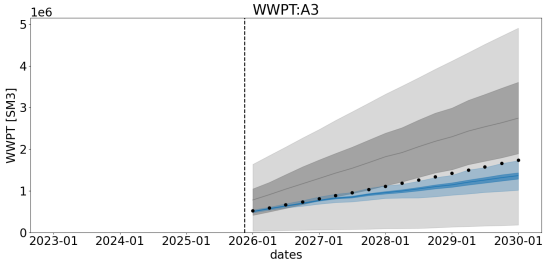

(c) Water Production for A-3

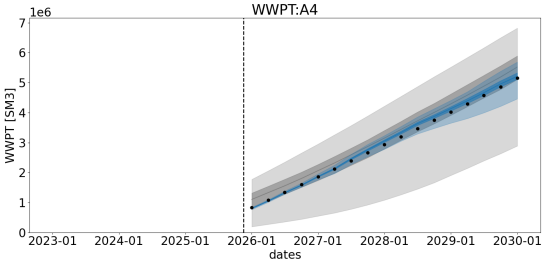

(d) Water Production for A-4

Figure 4.6: Plots showing water production for each producer. Black dots are 'truth-1' predictions, grey envelope is the prior ensemble, and blue envelope is posterior ensemble of DSI predictions. The darker shades within the envelope show 25-75 percentile of their respective ensembles.

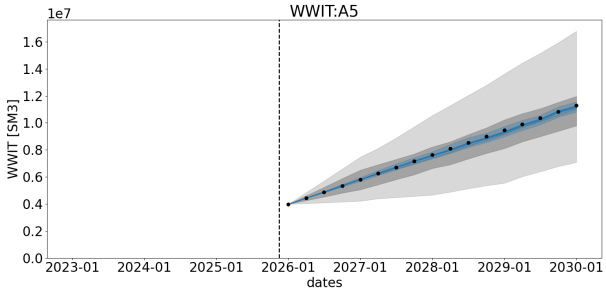

(a) Water injection for A5

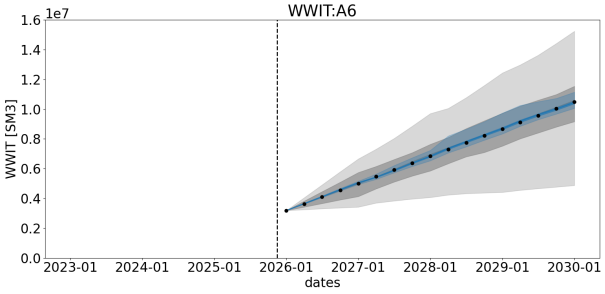

(b) Water injection for A6

Figure 4.7: Plots showing water injection of both the injectors. Black dots are 'truth-1' predictions, grey envelope is the prior ensemble, and blue envelope is posterior ensemble of DSI predictions. The darker shades within the envelope show 25-75 percentile of their respective ensembles.

4.2 Optimization Results: 'truth-1'

Figure 4.8 shows the comparison of the NPV values. The initial NPV value of the 'truth-1' is $3.28 billion. After implementing Everest-Eclipse optimization we achieve an NPV value of $3.41 bil-

lion, while Everest-DSI optimization yields an NPV of $3.39 billion. The values of the DSI optimisation are closely align with conventional optimization, thus again validating the accuracy of the DSI. Table 4.1 illustrates a little disparity between the $NPV_{\text{Everest-ECL}}$ and $NPV_{\text{Everest-DSI}}$. Such a small difference instills trust in using DSI for closed-loop reservoir management.

Figure 4.9 shows the initial and optimal injection rates of the injection wells that are determined using the conventional method and DSI, respectively. It is important to note that the optimal injection strategies are different, as expected. Table 4.2 presents the water injection rates of injectors for both the initial and optimal cases. Injection control variables across multiple optimization iterations over four time periods are provided in the appendix.

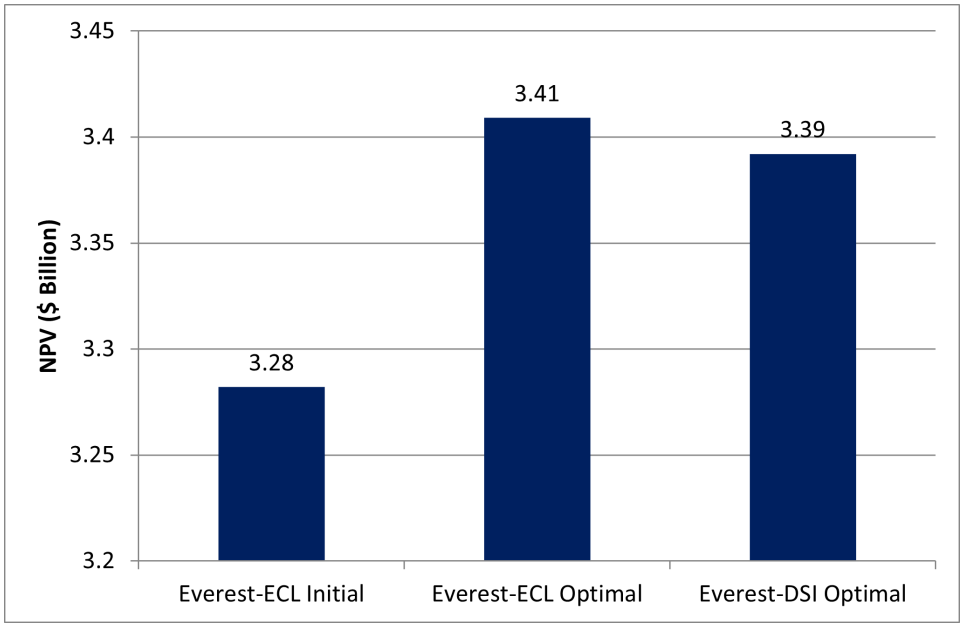

Figure 4.8: Chart showing NPV comparison between three scenarios

Table 4.1: NPV for initial and optimized cases for 'truth-1'.

Case	**NPV_{initial} [billion USD]**	**$NPV_{\text{Everest-ECL}}$ [billion USD]**	**$NPV_{\text{Everest-DSI}}$ [billion USD]**
'truth-1'	3.28	3.41	3.39

4.3 Sensitivity Results

This section presents and discusses results of sensitivity study on prior size, observation error and latent space on DSI framework as stated in Section 3.2.6 in Chapter3.

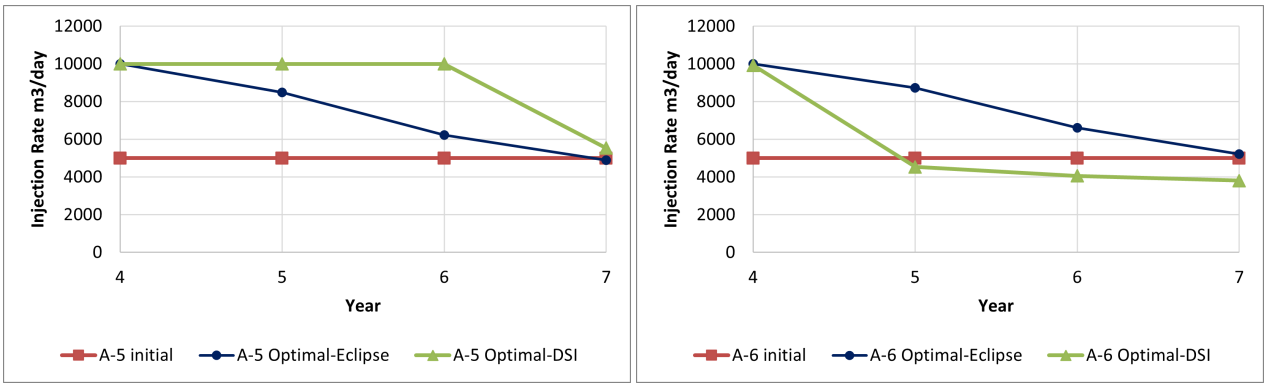

(a) Optimal Water Injection Rate for A5

(b) Optimal Water Injection Rate for A6

Figure 4.9: Plots show comparisons between control parameters for three cases for both injectors.

Table 4.2: Initial and optimal injection rates in m3/day for 'truth-1'.

Time	Initial		Optimal-Eclipse		Optimal-DSI	
year	A-5	A-6	A-5	A-6	A-5	A-6
4	5000	5000	10000	10000	10000	9924
5	5000	5000	8492	8739	10000	4539
6	5000	5000	6233	6610	10000	4063
7	5000	5000	4889	5217	5533	3807

4.3.1 Sensitivity on Prior Size

Three prior sizes were tested to find the optimum number of prior size needed for this study. The results of the cumulative oil production of well A-1 are shown in Fig. 4.10 with varying prior sizes. By referring to Fig. 4.10, it is evident that the results with the prior size of 500 and 1000 are satisfactory. However, for a prior size of 200, the 'truth' lies outside the posterior ensemble, rendering it less suitable for use in comparison to the other scenarios.

Prediction of cumulative water production from well A-1 is plotted in Fig. 4.11 and predicted cumulative injection from well A-5 is plotted in Fig. 4.12 for varying prior sizes. Water production and water injection exhibits identical trends to oil production, so confirming that the optimum prior size for this study is 500.

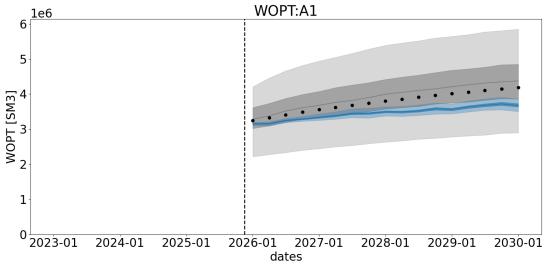

(a) Prior size 200

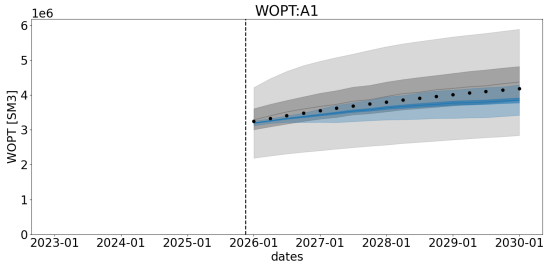

(b) Prior size 500

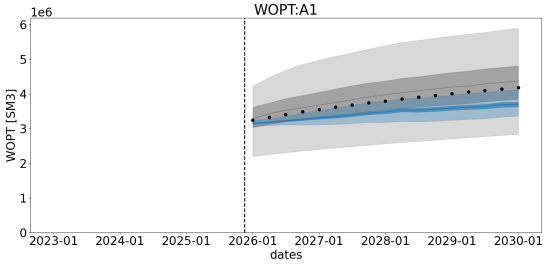

(c) Prior size 1000

Figure 4.10: Figures show oil production for producer A-1 for prior sizes of 200, 500 and 1000. Black dots are 'truth-1' predictions, grey envelope is the prior ensemble, and blue envelope is posterior ensemble of DSI predictions. The darker shades within the envelope show 25-75 percentile of their respective ensembles.

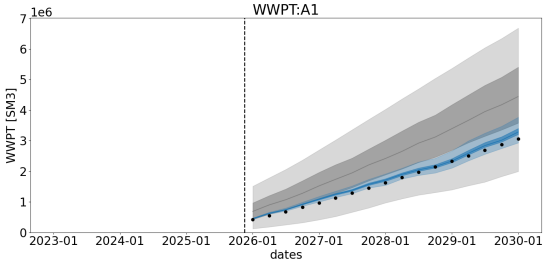

(a) Prior size 200

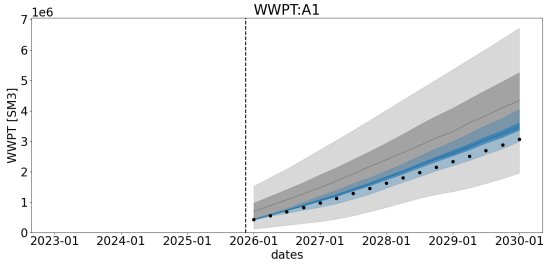

(b) Prior size 500

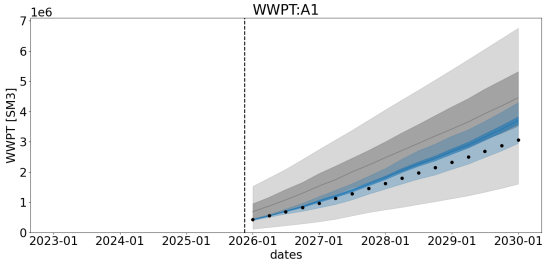

(c) Prior size 1000

Figure 4.11: Figures show water production for producer A-1 for prior sizes of 200, 500 and 1000. Black dots are 'truth-1' predictions, grey envelope is the prior ensemble, and blue envelope is posterior ensemble of DSI predictions. The darker shades within the envelope show 25-75 percentile of their respective ensembles.

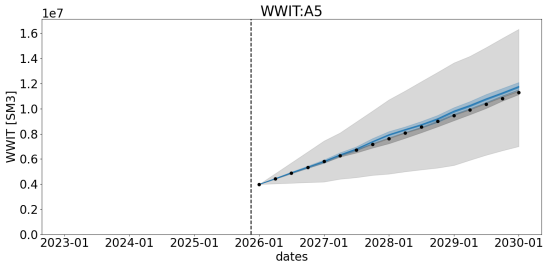

(a) Prior size 200

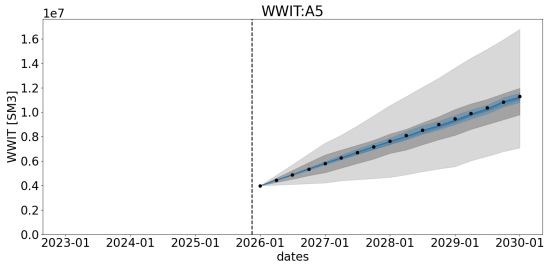

(b) Prior size 500

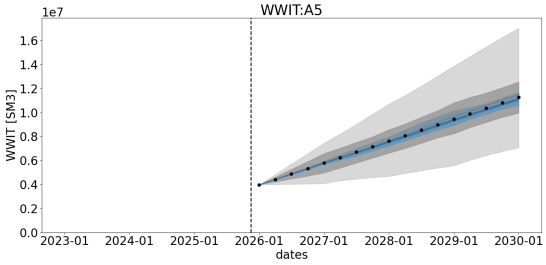

(c) Prior size 1000

Figure 4.12: Figures show water injection for injector A-5 for different latent space. Black dots are 'truth' predictions, grey envelope is the prior ensemble, and blue envelope is posterior ensemble of DSI predictions. The darker shades within the envelope show 25-75 percentile of their respective ensembles.

Prior size is one of the most critical features of the DSI, as predictions are conditioned based on this data. However, an excessively large prior size could adversely affect the efficiency of the DSI workflow. Hence, choosing the optimum size becomes crucial, which for this study has been determined to be 500.

4.3.2 Sensitivity on Observation Error

The HM values of well A-2 for oil production rate are displayed in Fig. 4.13, water rates are depicted in Fig. 4.14, and the BHPs are illustrated in Fig. 4.15 for different observation error. From these plots it is observed that the posterior ensemble coverage is inversely proportional to the observation error: it is smallest when the observation error is at its minimum and biggest when the observation error is at its maximum, among the cases. A similar trend is observed in Figs. 4.16 and 4.17, illustrating the predicted cumulative oil and water production of well A-2.

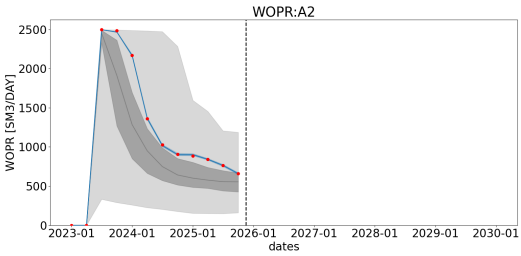

(a) Observation error of 1 bar and 5 Sm^3/day

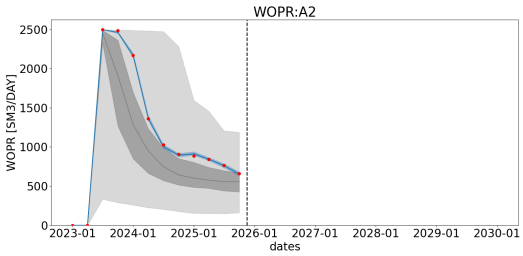

(b) Observation error of 2 bar and 10 Sm^3/day

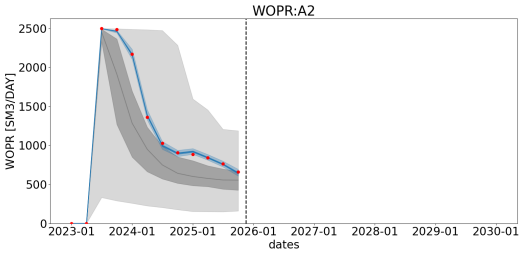

(c) Observation error of 4 bar and 20 Sm^3/day

Figure 4.13: Figures show oil production rate for producer A-2 for different sets of observation error. Red dots are observed data, grey envelope is the prior ensemble, and blue envelope is posterior ensemble of DSI predictions. The darker shades within the envelope show 25-75 percentile of their respective ensemble.

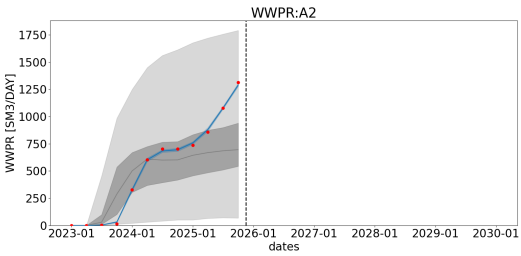

(a) Observation error of 1 bar and 5 Sm^3/day

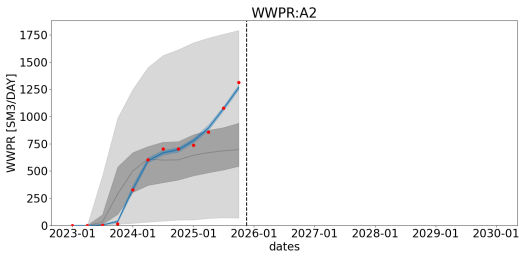

(b) Observation error of 2 bar and 10 Sm^3/day

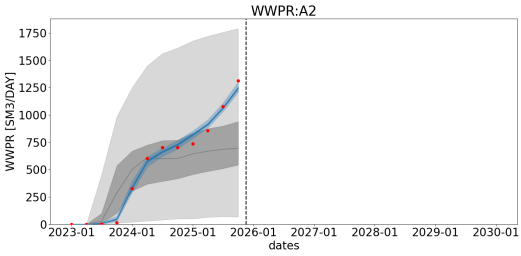

(c) Observation error of 4 bar and 20 Sm^3/day

Figure 4.14: Figures show water production rate for producer A-2 for different sets of observation error. Red dots are observed data, grey envelope is the prior ensemble, and blue envelope is posterior ensemble of DSI predictions. The darker shades within the envelope show 25-75 percentile of their respective ensemble.

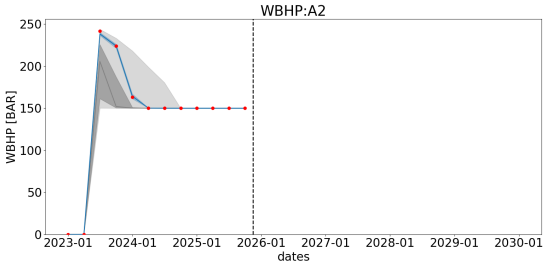

(a) Observation error of 1 bar and 5 Sm^3/day

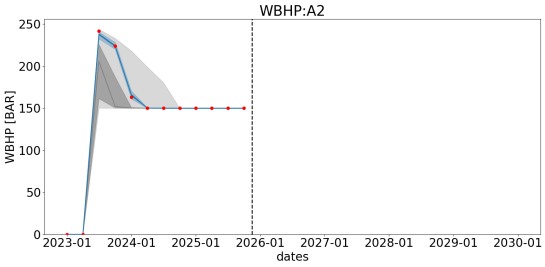

(b) Observation error of 2 bar and 10 Sm^3/day

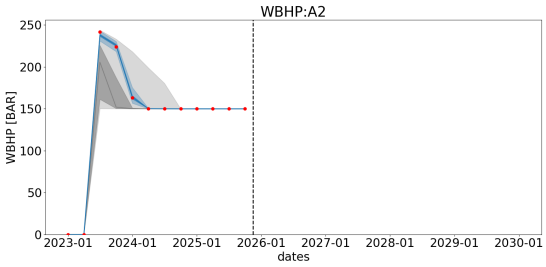

(c) Observation error of 4 bar and 20 Sm^3/day

Figure 4.15: Figures show BHP of producer A-2 for different sets of observation error. Red dots are observed data, grey envelope is the prior ensemble, and blue envelope is posterior ensemble of DSI predictions. The darker shades within the envelope show 25-75 percentile of their respective ensembles.

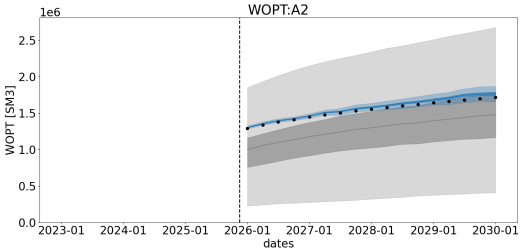

(a) Observation error of 1 bar and 5 Sm^3/day

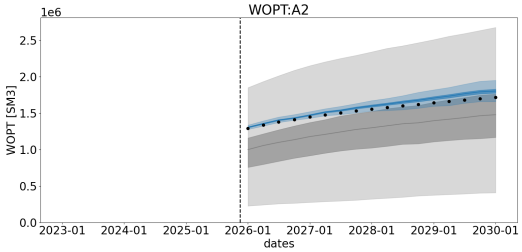

(b) Observation error of 2 bar and 10 Sm^3/day

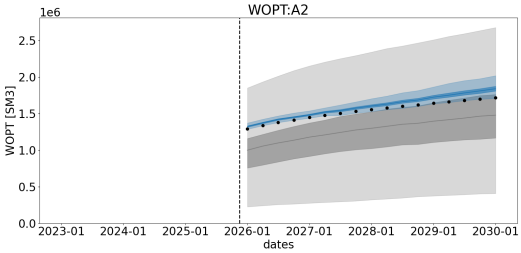

(c) Observation error of 4 bar and 20 Sm^3/day

Figure 4.16: Figures show oil production for producer A-2 for different sets of observation error. Black dots are 'truth-1' predictions, grey envelope is the prior ensemble, and blue envelope is posterior ensemble of DSI predictions. The darker shades within the envelope show 25-75 percentile of their respective ensemble.

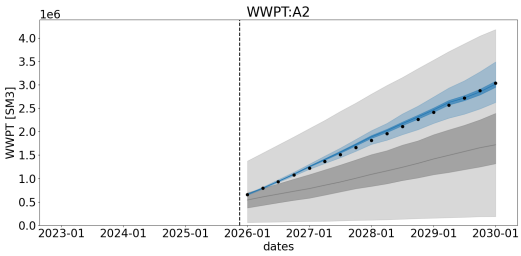

(a) Observation error of 1 bar and 5 Sm^3/day

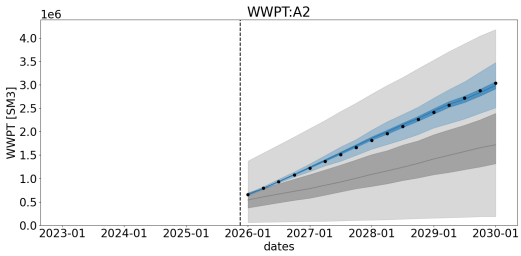

(b) Observation error of 2 bar and 10 Sm^3/day

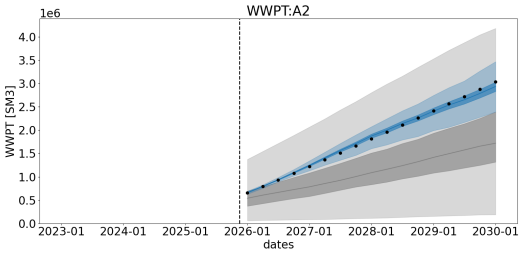

(c) Observation error of 4 bar and 20 Sm^3/day

Figure 4.17: Figures show water production for producer A-2 for different sets of observation error. Black dots are 'truth-1' predictions, grey envelope is the prior ensemble, and blue envelope is posterior ensemble of DSI predictions. The darker shades within the envelope show 25-75 percentile of their respective ensembles.

Observation error is a crucial parameter that enables us to account for the uncertainty present in the observed data. Given the characteristics of the HM Drogon ensemble, it is challenging to find the optimum tolerance for the observations. However, posterior ensemble of DSI follows the anticipated trend, with a narrower coverage in predictions when a lower tolerance is used and a broader coverage when a higher tolerance is used.

4.3.3 Sensitivity on Latent Space

Here, results from sensitivity in the latent space dimension are presented. The DSI posterior of historical oil rates, water rates, and BHPs is plotted in Figs. 4.18, 4.19 and 4.20 for the varying latent space dimensions, respectively. Based on these plots, all the values appear to be comparable, and solely on this information, one would select the latent space dimension of 100. However, when the total oil and water production are plotted for similar conditions, as presented in Figs. 4.21 and 4.22, it is evident that the latent space dimension of 100 does not yield an acceptable match with the 'truth-1' both for the cumulative oil (Fig.4.21(a)) and the cumulative water (Fig. 4.22(a)).

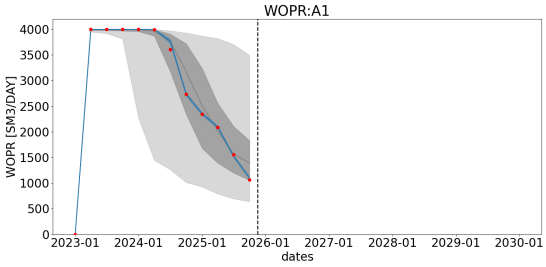

(a) Latent space 100

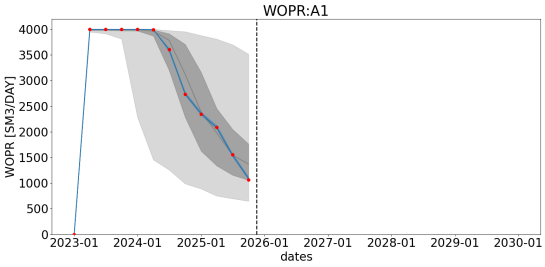

(b) Latent space 300

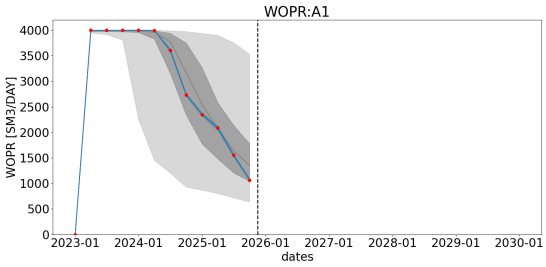

(c) Latent space 500

Figure 4.18: Figures show oil production rate for producer A-1 for different latent space. Red dots are observed data, grey envelope is the prior ensemble, and blue envelope is posterior ensemble of DSI predictions. The darker shades within the envelope show 25-75 percentile of their respective ensembles.

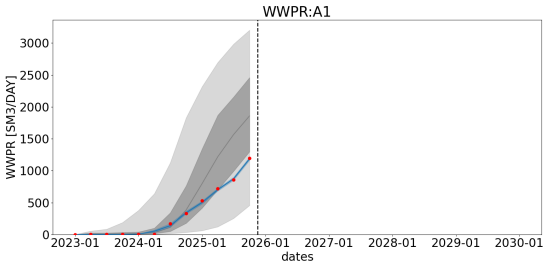

(a) Latent space 100

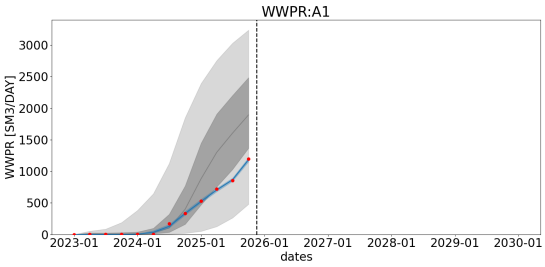

(b) Latent space 300

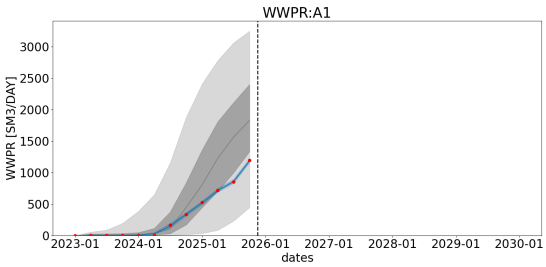

(c) Latent space 500

Figure 4.19: Figures show water production rate for producer A-1 for different latent space. Red dots are observed data, grey envelope is the prior ensemble, and blue envelope is posterior ensemble of DSI predictions. The darker shades within the envelope show 25-75 percentile of their respective ensembles.

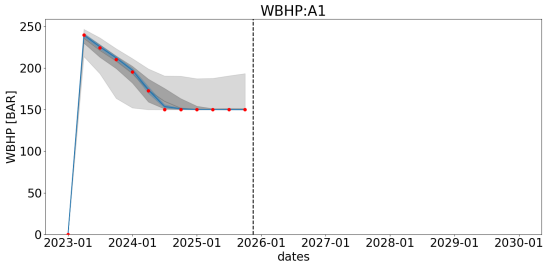

(a) Latent space 100

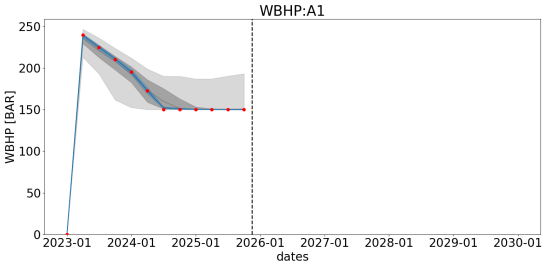

(b) Latent space 300

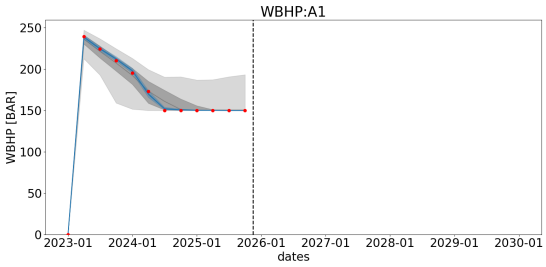

(c) Latent space 500

Figure 4.20: Figures show BHP for producer A-1 for different latent space. Red dots are observed data, grey envelope is the prior ensemble, and blue envelope is posterior ensemble of DSI predictions. The darker shades within the envelope show 25-75 percentile of their respective ensembles.

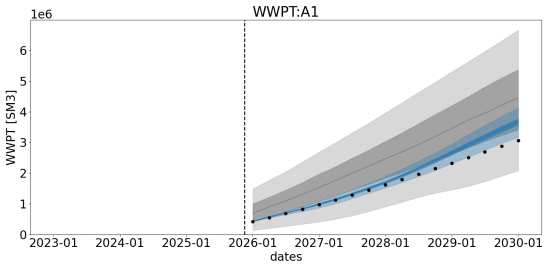

(a) latent space 100

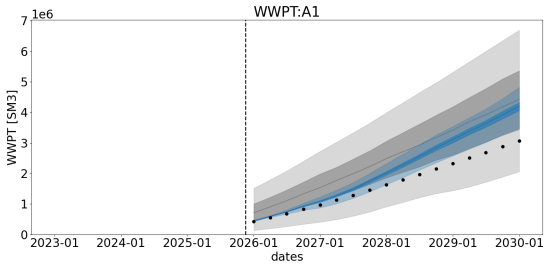

(b) latent space 300

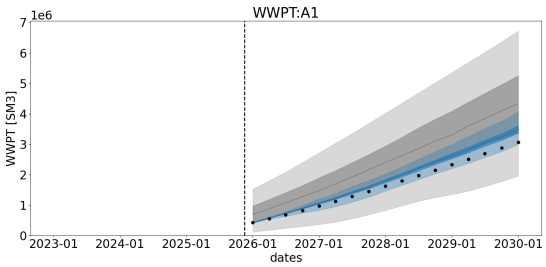

(c) Latent space 500

Figure 4.22: Figures show water production for producer A-3 for different latent space. Black dots are 'truth-1' predictions, grey envelope is the prior ensemble, and blue envelope is posterior ensemble of DSI predictions. The darker shades within the envelope show 25-75 percentile of their respective ensembles.

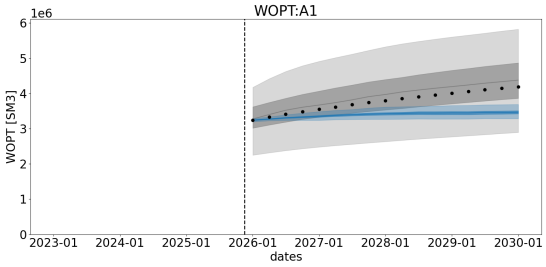

(a) latent space 100

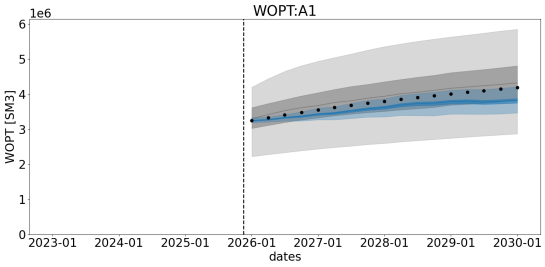

(b) latent space 300

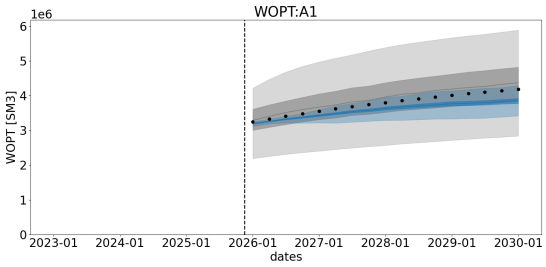

(c) Latent space 500

Figure 4.21: Figures show oil production for producer A-1 for different latent space. Black dots are 'truth-1' predictions, grey envelope is the prior ensemble, and blue envelope is posterior ensemble of DSI predictions. The darker shades within the envelope show 25-75 percentile of their respective ensembles.

Latent space dimension of 300 provides a satisfactory match for the cumulative oil production, as shown in Fig. 4.21(a) but is not valid for the cumulative water production, as depicted in Fig. 4.22(b). The latent space dimension of 500 matches the 'truth-1' as seen in Figs. 4.21(c) and 4.22(c) and hence the author has used the appropriate dimension of latent space for this study.

The dimension of the latent space influences the outcomes considerably. While a bigger dimension will impact computation efficiency, a smaller dimension may not yield adequate results due to the potential data loss during restructuring, as seen in the provided plots.

4.4 DSI Results Comparison for 'truth-1' and 'truth-2'

Figures 4.23(a) - 4.23(b) depicts the oil rate, Figs. 4.23(c) - 4.23(d) illustrate the water rates, and Figs. 4.23(e) - 4.23(f) represent the BHP of the 'truth-1' and the 'truth-2' respectively for well A-1. The figures clearly demonstrate the shift in the DSI posterior based on the different observed data ('truth-1' and 'truth-2'). When cumulative water injection, cumulative oil and water production for different 'truths' are plotted as seen in Figs. 4.24, 4.25, a comparable change in the predictions can be observed.

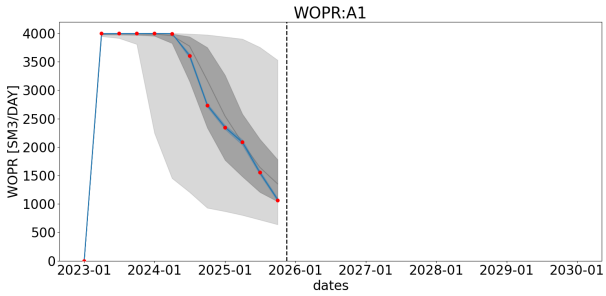

(a) ‘truth-1’

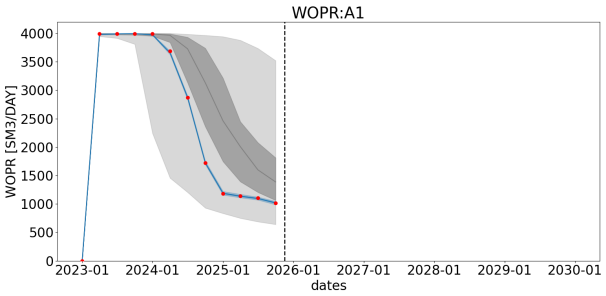

(b) ‘truth-2’

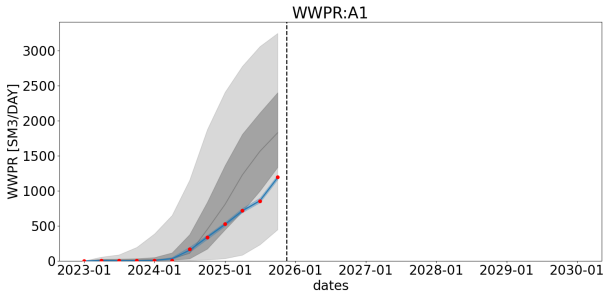

(c) ‘truth-1’

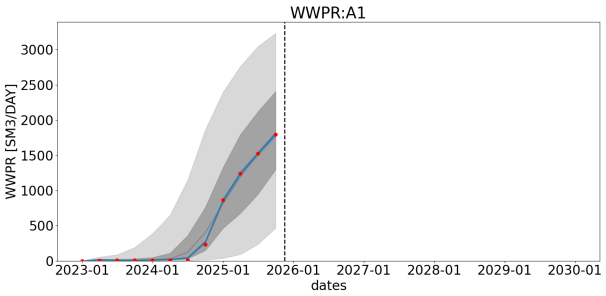

(d) ‘truth-2’

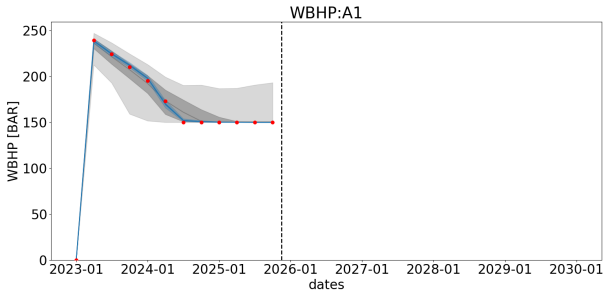

(e) ‘truth-1’

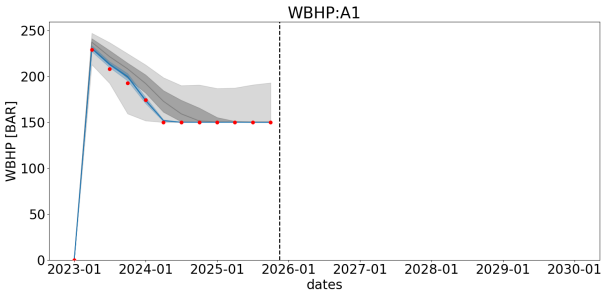

(f) ‘truth-2’

Figure 4.23: Figures show oil and water production rate and BHP of producer A-1 for different truth. Red dotted line represent the observed data, grey envelope represents the prior ensemble, dark grey area shows 25-75 percentile of prior ensemble. Blue envelope shows posterior ensemble.

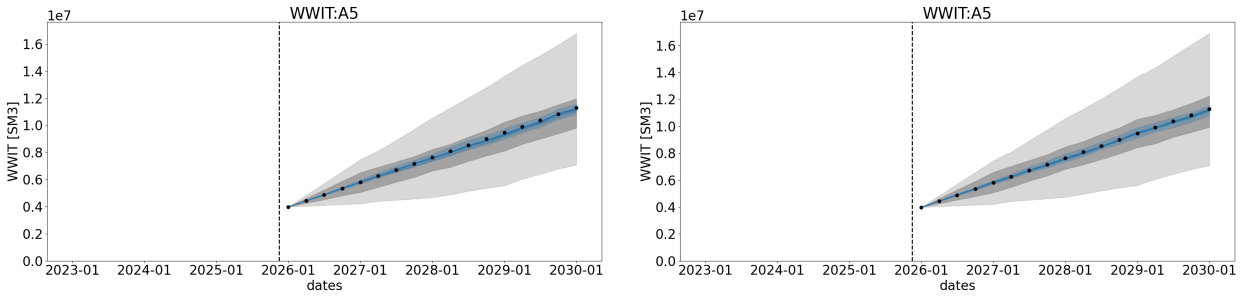

(a) 'truth-1'

(b) 'truth-2'

Figure 4.24: Figures show water injection of injector A5 for different truth. Black dots are 'truth' predictions, grey envelope is the prior ensemble, and blue envelope is posterior ensemble of DSI predictions. The darker shades within the envelope show 25-75 percentile of their respective ensembles.

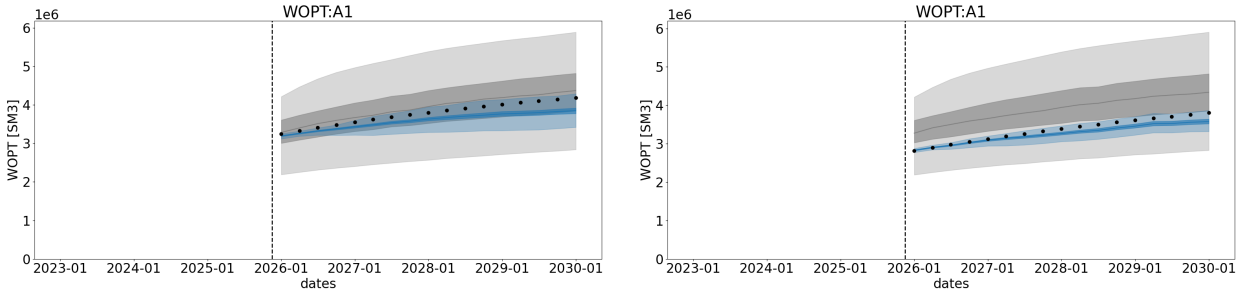

(a) 'truth-1'

(b) 'truth-2'

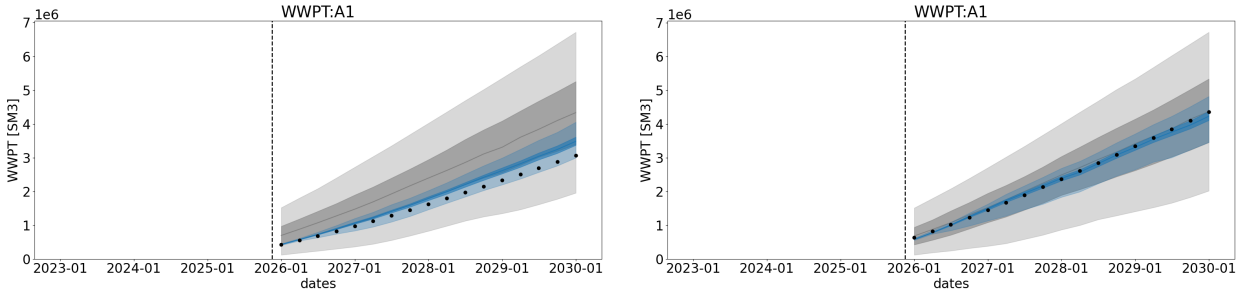

(c) 'truth-1'

(d) 'truth-2'

Figure 4.25: Figures show oil and water production of producer A-1 for different truth. Black dots are 'truth' predictions, grey envelope is the prior ensemble, and blue envelope is posterior ensemble of DSI predictions. The darker shades within the envelope show 25-75 percentile of their respective ensembles.

4.5 Optimization Results: 'truth-2'

Figure 4.26 shows the comparison of the NPV. The initial NPV of the 'truth-2' is $2.33 billion. After Everest-Eclipse optimization, an NPV value of $2.47 billion is achieved, on the contrary,

Everest-DSI optimization yields a NPV of $2.43 billion. The values of the DSI optimization are close to the conventional optimization, hence reaffirming the accuracy of the DSI workflow. Table 4.3 shows the difference between the $NPV_{\text{Everest-ECL}}$ and $NPV_{\text{Everest-DSI}}$.

Figure 4.27 displays the initial and optimal injection rates of the injection wells, that are determined using both the conventional approach and DSI. It is pertinent to note that the optimal injection strategies are different and are in line with expectations. Table 4.4 presents the water injection rates of injectors for the initial and optimal cases.

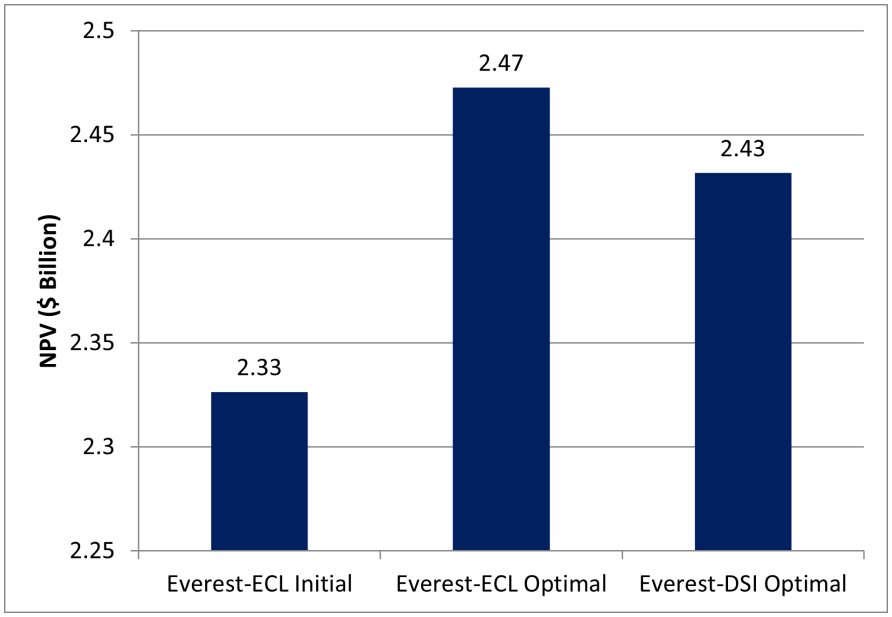

Figure 4.26: Chart showing NPV comparison between three scenarios

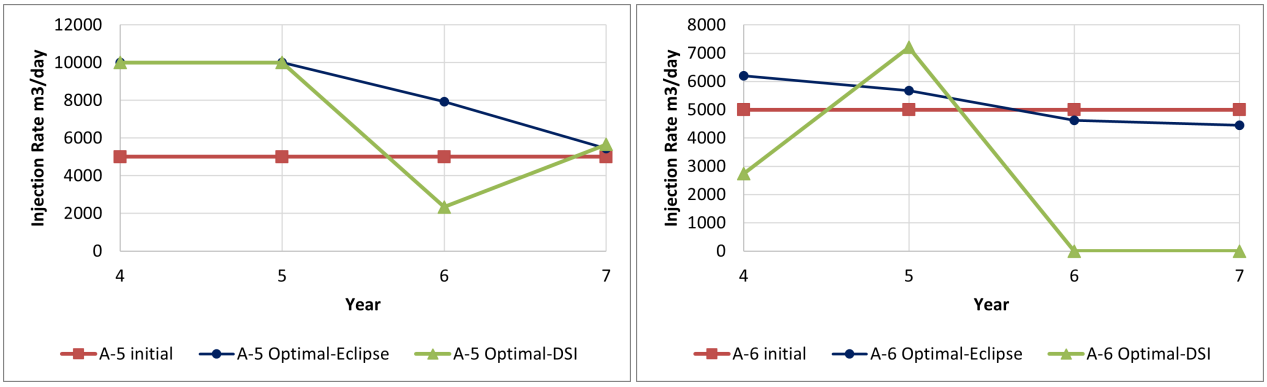

(a) Optimal Water Injection Rate for A5

(b) Optimal Water Injection Rate for A6

Figure 4.27: Plots shows comparison between optimal control parameters for three cases for both the injectors

Table 4.3: NPV for initial and optimized cases for 'truth-2'.

Case	**$NPV_{initial}$ [billion USD]**	**$NPV_{Everest\text{-}ECL}$ [billion USD]**	**$NPV_{Everest\text{-}DSI}$ [%]**
'truth-2'	2.33	2.47	2.43

Table 4.4: Initial and optimal injection rates in m3/day for 'truth-2'.

Time	**Initial**		**Optimal-Eclipse**		**Optimal-DSI**	
year	**A-5**	**A-6**	**A-5**	**A-6**	**A-5**	**A-6**
4	5000	5000	10000	6194	10000	2738
5	5000	5000	10000	5672	10000	7210
6	5000	5000	7918	4621	2342	0
7	5000	5000	5445	4446	5664	0

Chapter 5

Conclusions and Recommendations for Further Work

5.1 Conclusions

The study has been done to achieve the objectives outlined in section 1.2 and the results obtained have been discussed in detail in Chapter 4. The author applied the DSI methodology for robust reservoir optimization on the synthetic field, Drogon, chosen for its real field-like characteristics. The DSI framework was implemented based on the prior size of 500 members and the latent space dimension of 500. After generating the predictions from the DSI, optimization was performed, and the controls obtained were used to calculate the NPV of the 'truth-1'. Subsequently, the DSI NPV was compared with the optimized NPV of the 'truth-1' from the conventional methods. This exercise was replicated on a different truth ('truth-2') to establish the robustness of the DSI. It is known that the DSI is a computationally efficient method as compared to conventional methods, where models need to be updated for HM and future predictions. As anticipated, DSI proved to be a low-cost alternative to reservoir simulation, particularly in the context of ensemble based closed-loop reservoir management.

Duration of the study was 7 years out of which 3 year was the historical period and 4 year was the prediction period, and the result of the study demonstrated that DSI could be successfully implemented for the industrial application. DSI, when combined with an optimisation tool could prove to be a valuable asset in the ensemble based closed-loop reservoir management. Initially, the efficacy of DSI was evaluated by comparing NPV results with the traditional methods. Afterwards, optimal parameters for its functionality were established by conducting sensitivity anal-

ysis on different parameters such as prior size, observation error and latent space dimension. Robustness and adaptability of the DSI were demonstrated with the validation done through the 'truth-2' that proved to give comparable results to the conventional methods, similar to the 'truth-1'. From the discussion, the following conclusions can be drawn from this study:

- The DSI framework demonstrated a reasonable level of accuracy in predicting the relevant properties with fewer computations compared to traditional approaches.
- DSI provides flexibility to select the properties that are essential for the tasks, thereby reducing the computation time by predicting only the relevant properties.
- The author tested DSI workflow using ES-MDA and stochastic gradient optimization on a synthetic field, chosen for its real field like characteristics.
- The results suggest that prior size of 500 and latent space dimension of 500 are optimal for the study. However, due to the nature of the field data, sensitivity done on observation error proved inconclusive.

5.2 Recommendations for Further Work

DSI is a technique that has huge potential due to its ability to be fast, efficient, and versatile in handling diverse data sets. Following are some recommendations for further development of this technique.

- Despite possessing characteristics reminiscent to a real field, Drogon is nonetheless a synthetic field. DSI can be validated by a real field to further enhance its credibility.
- In reservoir modelling and simulation all the models are based on a single concept of facies, which are updated through data assimilation and then used for prediction. Due to the numerically extensive process, it is practically not feasible to have multiple facies concept for a single model. However, the DSI, which is computational savvy, can be used to test the different facies concept. This can assist in selection of the best facies concept for the field and has the potential to introduce a new perspective in the present modeling and simulation regime.
- Though autoencoders proved effective in handling complex datasets, but there is a chance of failure if the level of non-linearities increases. In such cases, it is advisable to explore alternative concepts such as Variational Autoencoders and Generative Adversarial Networks.

References

Bank, D., Koenigstein, N., Giryes, R., 2020. Autoencoders. URL: https://arxiv.org/abs/2003.05991.

Brouwer, D., Jansen, J.D., 2004. Dynamic optimization of waterflooding with smart wells using optimal control theory. SPE Journal 9, 391–402. doi:10.2118/78278-PA.

Chen, Y., Oliver, D.S., Zhang, D., 2009. Efficient Ensemble-Based Closed-Loop Production Optimization. SPE Journal 14, 634–645. URL: https://doi.org/10.2118/112873-PA, doi:10.2118/112873-PA, arXiv:https://onepetro.org/SJ/article-pdf/14/04/634/2555219/spe-112873-pa.pdf.

Emerick, A., Reynolds, A., 2013. Ensemble smoother with multiple data assimilation. Computers Geosciences 55, 3–15. doi:10.1016/j.cageo.2012.03.011.

Equinor, a. Drogon Conceptual Model. URL: https://webviz-subsurface-example.azurewebsites.net/drogon-conceptual-description.

Equinor, b. Equinor Everest Material. URL: https://fmu-docs.equinor.com/docs/everest/theory.html.

Evensen, G., 1994. Sequential data assimilation with a nonlinear quasi-geostrophic model using monte carlo methods to forecast error statistics. Journal of Geophysical Research: Oceans 99, 10143–10162. URL: https://agupubs.onlinelibrary.wiley.com/doi/abs/10.1029/94JC00572, doi:https://doi.org/10.1029/94JC00572, arXiv:https://agupubs.onlinelibrary.wiley.com/doi/pdf/10.1029/94JC00572.

Fonseca, R.M., Chen, B., Jansen, J.D., Reynolds, A., 2016. A stochastic simplex approximate gradient (stosag) for optimization under uncertainty: A stochastic simplex approximate gradient (stosag). International Journal for Numerical Methods in Engineering 109. doi:10.1002/nme.5342.

Haena, R.G., 2023. Integrated reservoir management GEO608. Lecture Notes GEO608.

Jiang, S., Sun, W., Durlofsky, L., 2020. A data-space inversion procedure for well control optimization and closed-loop reservoir management. Computational Geosciences 24. doi:10.1007/s10596-019-09853-4.

Lima, M., Emerick, A., Pico, C., 2020. Data-space inversion with ensemble smoother. Computational Geosciences 24. doi:10.1007/s10596-020-09933-w.

Michelucci, U., 2022. An introduction to autoencoders URL: https://arxiv.org/abs/2201.03898.

Oliver, D., Chen, Y., 2011. Recent progress on reservoir history matching: A review. Computational Geosciences 15, 185–221. doi:10.1007/s10596-010-9194-2.

Oliver, D., Reynolds, A., Liu, N., 2008. Inverse theory for petroleum reservoir characterization and history matching. Inverse Theory for Petroleum Reservoir Characterization and History Matching, by Dean S. Oliver, Albert C. Reynolds, Ning Liu. Cambridge: Cambridge University Press, 2008. doi:10.1017/CBO9780511535642.

Onwunalu, J., Durlofsky, L., 2010. Application of a particle swarm optimization algorithm for determining optimum well location and type. Computational Geosciences 14, 183–198. doi:10.1007/s10596-009-9142-1.

Rumelhart, D.E., Hinton, G.E., Williams, R.J., 1986. Learning internal representations by error propagation. URL: https://api.semanticscholar.org/CorpusID:62245742.

Sun, W., Durlofsky, L., 2017. A new data-space inversion procedure for efficient uncertainty quantification in subsurface flow problems. Mathematical Geosciences 49. doi:10.1007/s11004-016-9672-8.

Szklarz, S., Barros, E., 2022. Accelerating ensemble-based well control optimization with es-mda data-space inversion framework 2022, 1–11. URL: https://www.earthdoc.org/content/papers/10.3997/2214-4609.202244075, doi:https://doi.org/10.3997/2214-4609.202244075.

Appendix

Optimal Injection Control Parameters

Table A.1: Injection control variables attained from from Everest-ECL across multiple optimization iterations over four time periods for 'truth-1'

Well	A-5				A-6			
Year	4	5	6	7	4	5	6	7
Batch								
0	0.5000	0.5000	0.5000	0.5000	0.5000	0.5000	0.5000	0.5000
1	0.5110	0.5070	0.5029	0.5006	0.5082	0.5073	0.5037	0.4987
2	0.6086	0.5747	0.5226	0.4982	0.6032	0.5787	0.5329	0.5041
3	1.0000	0.8440	0.6191	0.4878	0.9913	0.8635	0.6587	0.5241
4	1.0000	0.8500	0.6212	0.4876	1.0000	0.8698	0.6616	0.5245
5	1.0000	0.8492	0.6233	0.4889	1.0000	0.8739	0.6610	0.5217

Table A.2: Injection control variables attained from from Everest-DSI across multiple optimization iterations over four time periods for 'truth-1'

Well	A-5				A-6			
Year	4	5	6	7	4	5	6	7
Batch								
0	0.5000	0.5000	0.5000	0.5000	0.5000	0.5000	0.5000	0.5000
1	0.5278	0.6194	0.5581	0.4948	0.5254	0.4956	0.5107	0.5110
2	0.7185	1.0000	0.7735	0.5039	0.6167	0.4627	0.5081	0.5121
3	0.8015	1.0000	0.8522	0.4751	0.6963	0.4702	0.5252	0.5219
4	0.9684	1.0000	1.0000	0.4269	0.8303	0.4867	0.5613	0.5375
5	1.0000	1.0000	1.0000	0.4171	0.8544	0.4912	0.5680	0.5404
6	1.0000	1.0000	1.0000	0.4372	0.8704	0.4853	0.5511	0.5307
7	1.0000	1.0000	1.0000	0.5608	1.0000	0.4423	0.4019	0.3712
8	1.0000	1.0000	1.0000	0.5231	1.0000	0.4836	0.4434	0.4139
9	1.0000	1.0000	1.0000	0.5485	1.0000	0.4557	0.4154	0.3851
10	1.0000	1.0000	1.0000	0.5575	1.0000	0.4459	0.4056	0.3750
11	1.0000	1.0000	1.0000	0.5599	1.0000	0.4433	0.4030	0.3723
12	1.0000	1.0000	1.0000	0.5606	1.0000	0.4425	0.4022	0.3715
13	1.0000	1.0000	1.0000	0.5607	1.0000	0.4423	0.4020	0.3713
14	1.0000	1.0000	1.0000	0.5608	1.0000	0.4423	0.4019	0.3712
15	1.0000	1.0000	1.0000	0.5608	1.0000	0.4423	0.4019	0.3712
16	1.0000	1.0000	1.0000	0.5608	1.0000	0.4423	0.4019	0.3712
17	1.0000	1.0000	1.0000	0.5608	1.0000	0.4423	0.4019	0.3712
18	1.0000	1.0000	1.0000	0.5608	1.0000	0.4423	0.4019	0.3712
19	1.0000	1.0000	1.0000	0.5533	0.9924	0.4539	0.4063	0.3807

Table A.3: Injection control variables attained from from Everest-ECL across multiple optimization iterations over four time periods for 'truth-2'

Well	A-5				A-6			
Year	4	5	6	7	4	5	6	7
Batch								
0	0.5000	0.5000	0.5000	0.5000	0.5000	0.5000	0.5000	0.5000
1	0.5154	0.5105	0.5060	0.5018	0.5007	0.5020	0.5001	0.4974
2	0.6063	0.5834	0.5434	0.5089	0.5173	0.5114	0.4935	0.4921
3	0.6970	0.6559	0.5834	0.5162	0.5340	0.5207	0.4875	0.4854
4	0.7928	0.7343	0.6267	0.5232	0.5537	0.5312	0.4808	0.4761
5	0.8941	0.8179	0.6694	0.5324	0.5716	0.5410	0.4749	0.4673
6	1.0000	0.9015	0.7141	0.5398	0.5916	0.5517	0.4696	0.4605
7	1.0000	0.9200	0.7262	0.5405	0.5959	0.5543	0.4691	0.4582
8	1.0000	1.0000	0.7795	0.5438	0.6170	0.5642	0.4659	0.4460
9	1.0000	1.0000	0.7918	0.5445	0.6194	0.5672	0.4621	0.4446

Table A.4: Injection control variables attained from from Everest-DSI across multiple optimization iterations over four time periods for 'truth-2'

Well	A-5				A-6			
Year	4	5	6	7	4	5	6	7
Batch								
0	0.5000	0.5000	0.5000	0.5000	0.5000	0.5000	0.5000	0.5000
1	0.5108	0.5306	0.2964	0.3862	0.2523	0.7006	0.0539	0.2192
2	0.5587	0.5949	0.2911	0.4052	0.2570	0.6973	0.0000	0.1974
3	0.8991	1.0000	0.2418	0.5337	0.2748	0.7220	0.0000	0.0410
4	1.0000	1.0000	0.2343	0.5664	0.2738	0.7211	0.0000	0.0002
5	1.0000	1.0000	0.2342	0.5664	0.2738	0.7210	0.0000	0.0000